Article

Cell Stem Cell

Integrin α7 Is a Functional Marker and Potential Therapeutic Target in Glioblastoma

Graphical Abstract

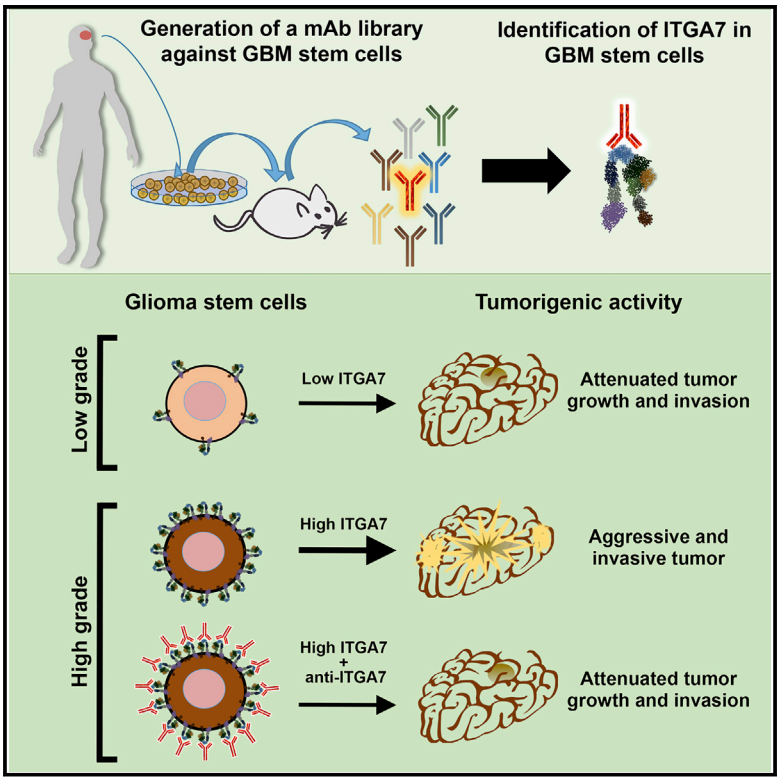

Highlights

- Hybridoma library screening highlights integrin α7 as a glioblastoma antigen
- Knockdown of integrin α7 impairs growth and survival of glioblastoma stem cells
- High integrin α7 expression correlates with poor prognostic outcomes in patients
- An antibody against integrin α7 suppresses tumor growth and invasion

Authors

Tobias L. Haas, Maria Rita Sciuto, Lidia Brunetto, ..., Lucia Ricci-Vitiani, Roberto Pallini, Ruggero De Maria

Correspondence

thaas0@gmail.com (T.L.H.), ruggero.demaria@unicatt.it (R.D.M.)

In Brief

Haas et al. identify integrin α7 as a functional marker of glioblastoma stem cells by screening a monoclonal antibody library generated against primary glioblastoma (GBM) cells. Functional experiments in culture and in vivo show that the targeting of integrin α7 has potential as a therapeutic avenue for treating this aggressive disease.

Haas et al., 2017, Cell Stem Cell *21*, 1–16
July 6, 2017 © 2017 Elsevier Inc.
http://dx.doi.org/10.1016/j.stem.2017.04.009

CellPress

Please cite this article in press as: Haas et al., Integrin α7 Is a Functional Marker and Potential Therapeutic Target in Glioblastoma, Cell Stem Cell (2017), http://dx.doi.org/10.1016/j.stem.2017.04.009

Cell Stem Cell
Article

Integrin α7 Is a Functional Marker and Potential Therapeutic Target in Glioblastoma

Tobias L. Haas,[1,2,3,*] Maria Rita Sciuto,[2] Lidia Brunetto,[2,8] Cecilia Valvo,[1,2,3,8] Michele Signore,[2] Micol E. Fiori,[1,2,3] Simona di Martino,[2,3] Stefano Giannetti,[4] Liliana Morgante,[4] Alessandra Boe,[2] Michele Patrizii,[2] Uwe Warnken,[5] Martina Schnölzer,[5] Andrea Ciolfi,[2,6] Chiara Di Stefano,[2] Mauro Biffoni,[2] Lucia Ricci-Vitiani,[2] Roberto Pallini,[7,9] and Ruggero De Maria[1,3,9,10,*]

[1]Institute of General Pathology, Università Cattolica del Sacro Cuore and Fondazione Policlinico Universitario A. Gemelli, 00168 Rome, Italy
[2]Department of Oncology and Molecular Medicine – Istituto Superiore di Sanità, 00161 Rome, Italy
[3]National Cancer Institute Regina Elena, 00144 Rome, Italy
[4]Institute of Anatomy and Cell Biology, Università Cattolica del Sacro Cuore, 00168 Rome, Italy
[5]Functional Proteome Analysis, German Cancer Research Center, 69120 Heidelberg, Germany
[6]Food and Nutrition Research Center, CREA, 00178 Rome, Italy
[7]Institute of Neurosurgery, Università Cattolica del Sacro Cuore, 00168 Rome, Italy
[8]These authors contributed equally
[9]These authors contributed equally
[10]Lead Contact
*Correspondence: thaas0@gmail.com (T.L.H.), ruggero.demaria@unicatt.it (R.D.M.)
http://dx.doi.org/10.1016/j.stem.2017.04.009

SUMMARY

Functionally relevant markers of glioblastoma stem-like cells (GSCs) have potential for therapeutic targeting to treat this aggressive disease. Here we used generation and screening of thousands of monoclonal antibodies to search for receptors and signaling pathways preferentially enriched in GSCs. We identified integrin α7 (ITGA7) as a major laminin receptor in GSCs and in primary high-grade glioma specimens. Analyses of mRNA profiles in comprehensive datasets revealed that high ITGA7 expression negatively correlated with survival of patients with both low- and high-grade glioma. In vitro and in vivo analyses showed that ITGA7 plays a key functional role in growth and invasiveness of GSCs. We also found that targeting of ITGA7 by RNAi or blocking mAbs impaired laminin-induced signaling, and it led to a significant delay in tumor engraftment plus a strong reduction in tumor size and invasion. Our data, therefore, highlight ITGA7 as a glioblastoma biomarker and candidate therapeutic target.

INTRODUCTION

Glioblastoma (GBM) is the most aggressive and frequent form of malignant brain tumor in adults. Its fast growth rate, high invasive potential, and therapy resistance result in a very poor prognosis with a median survival of about 14 months (Johnson and O'Neill, 2012). There is accumulating evidence supporting that GBM growth is driven by a subset of cells displaying an undifferentiated phenotype and endowed with stem cell properties, such as unlimited self-renewal, high drug resistance, and multilineage differentiation (Cheng et al., 2013; Ricci-Vitiani et al., 2010; Son et al., 2009; Wang et al., 2010). Intense efforts are being made to identify GBM surface molecules and pathways that can be exploited for therapeutic targeting. Due to the heterogeneity of GBM, several surface markers have been proposed to identify GBM stem-like cells (GSCs) (Binda et al., 2012; Day et al., 2013; Lathia et al., 2010; Singh et al., 2004; Son et al., 2009). These markers seem valid only for subsets of GBM, and no generally accepted universal marker for highly malignant GSCs has been defined yet. Propagation of primary GBM cultures as neurospheres appears to be a valuable tool to identify, characterize, and target GBM-initiating or -propagating cells (Vescovi et al., 2006). Although a number of studies have exploited these primary tumorigenic cells to increase the understanding of GBM biology, the repertoire of their functional surface molecules has not been systematically explored.

Here we generated random antibodies preferentially reacting with primary GSCs as compared to their differentiated, less tumorigenic counterpart. This unbiased approach led to the isolation of an mAb recognizing and blocking integrin α7 (ITGA7) function. Like ITGA3 and ITGA6, ITGA7 binds several laminin isoforms in conjunction with the integrin β1 subunit (ITGB1) (von der Mark et al., 2002). Its physiological function appears to preferentially involve the skeletal muscle integrity (Hayashi et al., 1998; Mayer et al., 1997), but it was also described as tumor and metastasis suppressor in prostate cancer and melanoma, respectively (Ren et al., 2007; Ziober et al., 1999). In contrast, we show that ITGA7 is aberrantly expressed in aggressive gliomas and acts as a key functional receptor in GSCs, allowing for AKT activation and invasion. ITGA7 high-expressing cells from freshly dissociated tumors are enriched in tumor-initiating cells, which exploit this integrin for promoting tumor growth and malignant invasion. Although additional laminin-binding integrins may contribute to increase the GSC aggressiveness, ITGA7 is overexpressed in gliomas from patients with particularly poor survival, and it appears to play a significantly stronger role in tumor progression.

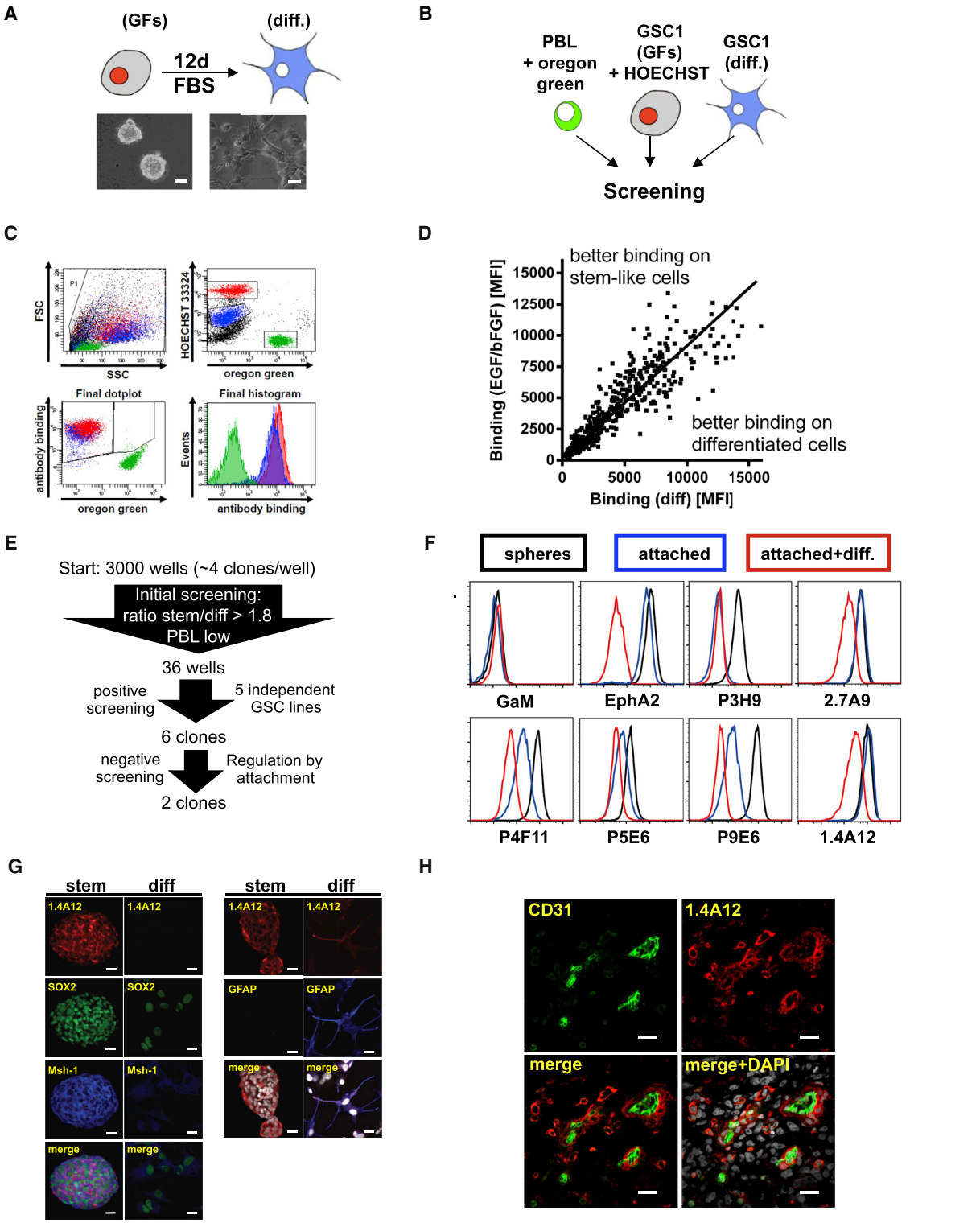

Figure 1. Isolation of Antibody-Recognizing Surface Antigens Preferentially Expressed in GSCs

(A) Microscopic pictures comparing undifferentiated and serum-differentiated primary GBM cells (scale bar, 50 μm). See also Figures S1A and S1B.

(B) Labeling used for the high-throughput screening (PBL, peripheral blood lymphocyte).

(C) Representative result of the flow cytometric analyses obtained by the high-throughput screening. The red and blue colors represent undifferentiated (HOECHST-positive) and differentiated primary GSC1 cells, respectively. The green color represents Oregon green-stained PBLs.

(legend continued on next page)

RESULTS

Generation and Screening of a Hybridoma Library Raised against GSC Surface Antigens

To identify novel surface markers expressed in GSCs, we produced an mAbs library using well-characterized (Ricci-Vitiani et al., 2008, 2010) primary GBM-derived neurospheres (GSC1) at early passages as immunogen. The neurospheres (Figure 1A) expressed high levels of nestin (Figure S1A); contained proliferating (Figures S1B and S1C), self-renewing cells (Figure S1D); and formed highly infiltrative tumors in mouse brains (Ricci-Vitiani et al., 2010). Upon cancer stem cell (CSC) differentiation (Figure 1A), nestin was downregulated, GFAP was induced (Figure S1A), proliferation slowed down (Figures S1B and S1C), and self-renewal capacity was lost (Figure S1D). We immunized BALB/c mice with viable GSC1 cells, and we generated hybridomas by performing three fusions that were directly cloned, summing up in 3,000 wells with 12,000 individual clones. For high-throughput flow cytometric screening, GSC1 neurospheres were labeled with HOECHST 33342, and they were mixed with unlabeled, differentiated isogenic cells and peripheral blood leukocytes (PBLs) labeled with cell tracker Oregon green (Figure 1B). This allowed us to analyze the antibody binding in three different cell populations (Figure 1C). We found antibody surface binding in 28.3% of the samples. To ensure a fast and stringent selection of antibodies preferentially binding on undifferentiated GSCs, but not binding widespread human surface molecules, we chose only hybridomas with no or low affinity toward PBL and a binding ratio undifferentiated/differentiated GSC1 $\geq$1.8 for further analysis (Figures 1D and 1E). In a rescreening, we confirmed binding in 26 cases. We assumed that we lost functional hybridomas due to genomic instability induced by the fusion. Because of the heterogeneity in GBM, only a few supernatants reacted positively with the majority of GSCs tested. Thus, we concentrated our efforts on six hybridoma clones that recognized at least five additional independent primary GSC cultures (data not shown).

To test if spheroid versus isogenic adherent culture influences the expression of the antigens, we compared antibody binding on undifferentiated cells grown in spheres or on a laminin matrix as monolayer (Pollard et al., 2009) with in-vitro-differentiated cells. As expected, the binding of all selected antibodies was reduced upon cell differentiation. However, we observed a significant reduction in the binding of four of six antibodies to cells cultivated on laminin, suggesting a major impact of the adhesion status on the expression of the mAb antigens. In contrast, the binding of mAb 2.7A9 and 1.4A12 was like the stem cell marker EphA2, not altered by adhesion (Figure 1F), indicating that their respective antigens might be potential markers for undifferentiated GSCs. Interestingly, both antibodies displayed weak or no binding on conventional ATCC brain tumor cell lines (Figure S1E). Finally, we focused our attention on the hybridoma clone 1.4A12, which showed a more robust binding in a panel of primary GBM lines (Figure S1E). We verified the localization of the antigen on the cell surface of undifferentiated GSCs, its weak expression in differentiated cells, and the correlation with other stem cell markers (Figure 1G). Immunofluorescence analysis of GBM patient samples revealed a general enrichment of the mAb 1.4A12 antigen expression in the area around the vessels (Figures 1H and S1F). In summary, by using this unbiased screening for monoclonal antibodies recognizing surface molecules on GBM cells with a stem-like phenotype, we isolated mAb 1.4A12 that preferentially stains GBM cells in the perivascular regions.

The mAb 1.4A12 Antigen Is Co-expressed with Markers of Undifferentiated GBM Cells, and It Selects for More Tumorigenic Cells

To confirm that mAb 1.4A12 binds to less differentiated, potentially more aggressive GBM cells in the tumor bulk, we performed fluorescence-activated cell sorting (FACS)-assisted cell separation of GFP-transduced cells from xenografts obtained from primary spheroid GBM cultures. In contrast to primary patient-derived tumors, the GFP expression in the xenograft-derived cells ensured the exclusion of debris and potential non-tumor cells from further downstream analysis, thus reducing the experimental bias in the cell-sorting experiments. Tumor cells freshly dissociated from xenografts generated by three different spheroid GBM cultures showed a co-expression of the mAb 1.4A12 antigen and established GBM stem cell surface markers, such as CD44, integrin alpha 6, and EphA2 (Figure 2A).

Upon cell sorting, we observed a considerable difference in sphere formation between mAb 1.4A12 dim and bright cells, the latter being far more efficient (Figure 2B). We found that several GSC and proliferation-associated transcripts, such as EphA2, EphA3, FGF1, nestin, MELK1, CDK1, cyclins, and Ki67, were preferentially expressed by the mAb 1.4A12 high-expressing cell fraction. On the contrary, genes known to be upregulated during neuronal differentiation were stronger expressed in cells with low mAb 1.4A12 binding (Figures 2C, S2A, and S2B). These results suggested that cells expressing high levels of the mAb 1.4A12 antigen could have a potentially less differentiated and more aggressive phenotype. Indeed, we observed that mAb 1.4A12 high cells obtained from xenografts of three independent patients grew significantly faster in vitro (Figure 2D), and they contained a significantly higher number of clonogenic cells

(D) Results of the screening for immunoreactions of the hybridoma supernatants. Plotted is the mean fluorescence intensity (MFI) for stem-like versus differentiated GSC1.

(E) Scheme of the high-throughput screening strategy.

(F) Verification of antigen down-modulation by differentiation. GSC1 cells were grown under spheroid conditions (spheres, black), on laminin in the presence of GF (attached, blue) or in vitro differentiated (red). Flow cytometric analyses for the antibodies and hybridoma supernatants (SNs) indicated were performed.

(G) Immunofluorescence analysis of GSC1 cultivated under stem cell conditions (stem) or upon in vitro differentiation (diff) with the antibodies indicated. DAPI is visualized in white.

(H) Representative immunofluorescence staining of a primary frozen GBM stained for the vascular marker CD31 (green), 1.4A12 antibody (red), and DAPI (white). Scale bar, 40 μm (G and H).

See also Figure S1F.

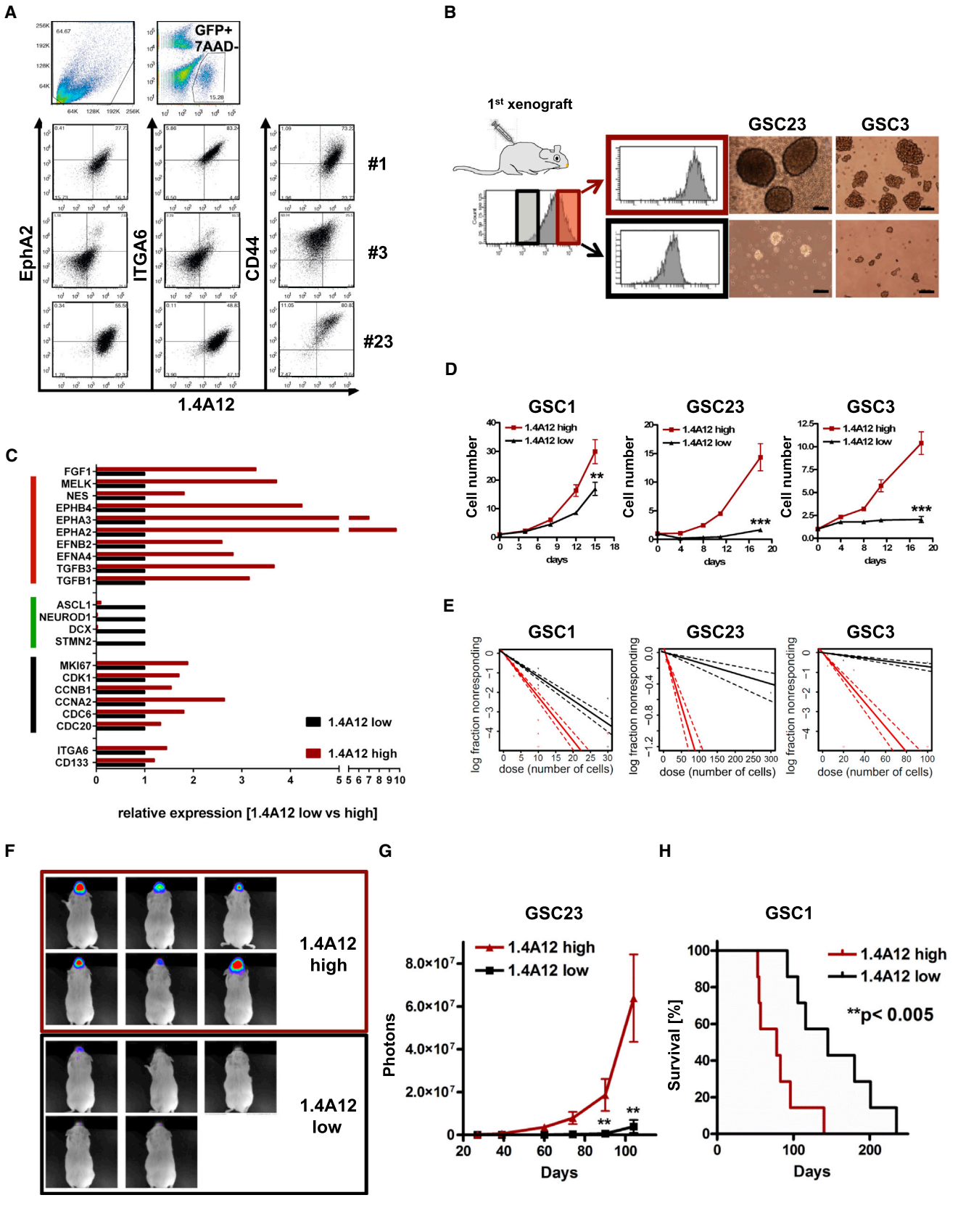

(legend on next page)

(Figures 2E and S2C). By performing orthotopic implantations of xenograft-derived sorted cells in a second recipient mouse, we also verified that high antigen-expressing cells grew significantly faster (Figures 2F and 2G) and behaved more aggressively in vivo (Figure 2H). Thus, GBM cells expressing high levels of the mAb 1.4A12 antigen are enriched in aggressive, undifferentiated GSCs.

Identification of ITGA7 as mAb 1.4A12 Antigen

The strong surface binding of mAb 1.4A12 to GSC1 enabled us to biochemically purify and identify the antigen by mass spectrometric analysis. Using immunoprecipitation from cell surface biotinylated GSC1, we determined a molecular weight of ~100–110 kDa for the mAb 1.4A12 antigen (Figure 3A). We also detected a protein signal at the same molecular weight in silver- and Coomassie-stained SDS-PAGE gels (Figures 3A and S3A). The bands were excised from the gel, and tandem mass spectrometric analysis was performed. Among the 30 most abundant proteins detected (Table S1), ITGA7 and ITGB1 were the only two surface proteins with high sequence coverage (Figures S3B and S3C). We confirmed that ITGA7 and ITGB1 are co-immunoprecipitated by both 1.4A12 and ITGB1 mAbs (Figure 3B), indicating that mAb 1.4A12 recognized ITGA7, ITGB1, or the heterodimer of both.

To prove which protein was the antigen, we transduced murine L929 cells with human ITGA7 cDNA. This resulted in the binding of mAb 1.4A12 on the cell surface (Figure 3C). In contrast, the expression of human ITGB1 cDNA did not lead to mAb binding to L929. We confirmed these data with the human GBM cell line T98G (Figure S3D). Since also the small hairpin RNA (shRNA)-mediated knockdown of ITGA7 (ITGA7-KD) in different GSCs led to a reduction in antibody surface binding (Figure S3E), we assumed that ITGA7 is the surface antigen recognized by mAb 1.4A12 that we thereafter referred to as anti-ITGA7. We then confirmed our FACS results, and we observed the down-modulation of ITGA7 upon differentiation with a commercially available ITGA7 antibody by western blot (Figure S3F). After finding that anti-ITGA7 is specific for the human protein (Figure S3G), we tested if it might also have some biological activity. We generated MCF7 cells stably expressing ITGA7 (Figure 3D), and we found that anti-ITGA7 inhibits the binding of these cells to laminin, the natural substrate of ITGA7, in a concentration-dependent manner (Figure 3E). In conclusion, these results showed that our antibody is not only able to select ITGA7-expressing cells but also blocks ITGA7 function by interfering with the ITGA7-laminin binding.

ITGA7 Is Crucial for Proliferation and Clonogenic Survival of GBM In Vitro and In Vivo

To get a more comprehensive idea about the molecular pathways influenced by ITGA7, we tested for more than 70 (phospho-) proteins involved in tumor cell proliferation and survival in ITGA7 pro- and deficient GSCs by reverse-phase protein array (RPPA) (Marziali et al., 2016). The RPPA analysis revealed that GSCs obtained from different patients showed marked differences in their basal pathway activation patterns already in the control cells (Figure 3F). To reduce the complexity, we compared the activation of pathways upon ITGA7-KD within the individual GSCs (Figure 3G). In this screening, we found no consistent differences in the activation pattern of proteins playing roles in apoptosis and Wnt, mitogen-activated protein kinase (MAPK), and nuclear factor κB (NF-κB) signaling. Interestingly, within the MAPKs, only phosphorylated p38 was downregulated upon ITGA7-KD in all cells tested (Figure 3G).

Analyzing other pathways, the most robust differences between the control and ITGA7-depleted cells were observed in the analyses of cell cycle-regulating proteins and the phosphorylation states of protein involved in the PI3K/AKT pathway (Figure 3G). Western blot analysis confirmed the RPPA data and showed a decrease of phosphorylated AKT and p38 in cells lacking ITGA7 (Figures 4A and S4A). In addition to the attenuation of steady-state phosphorylation levels, ITGA7-KD was able to reduce AKT activation upon stimulation with laminin (Figure 4A). This inhibition was also observed by using anti-ITGA7 antibody, although it was less effective compared to the genetic depletion. Of note, anti-ITGA7 treatment had only a marginal effect on p38 activity (Figure S4B). Upon ITGA7-KD, we also found reduced levels of phosphorylated, inactive FOXO3a, together with FoxO1, a well-established AKT target protein and regulator of FoxM1 expression. This may explain the low levels of FoxM1 (Figure 4B) and its target genes active in cell-cycle progression, DNA repair, and invasion (Figure 4C) in ITGA7-KD cells. In cells

Figure 2. Isolation of Antibody-Recognizing Surface Antigens Preferentially Expressed in GSCs

(A) Flow cytometric analyses of freshly isolated xenografts obtained from GFP-positive primary GBM lines from three independent GBM patients. Shown are the gating strategy and the co-staining with mAb 1.4A12 and established CSC markers CD44, ITGA6, and EphA2.

(B) Sorting strategy used to investigate the biological functions of cells expressing high versus low levels of mAb 1.4A12 antigen. Shown are representative post-sorting controls and microscopic pictures of the spheres formed 3 weeks after the sorting of cells (scale bar, 100 μm).

(C) The mAb 1.4A12 high- and low-binding cells derived from fresh GSC1 xenografts were sorted, and qPCR for genes with functions in CSC biology (red line), proliferation (black line), and neuronal differentiation (green line) was performed. Shown is the relative expression of the indicated mRNAs compared to the mAb 1.4A12 dim cell population. The biological replicates are shown in Figure S2.

(D) Cells derived from xenografts of three independent GBM patients were sorted as in (B). To determine the cell proliferation, cell numbers were compared to day 0 and the fold increase was plotted. Shown are the average and SD of at least three replicates (**$p < 0.01$ and ***$p < 0.001$, Student's t test).

(E) The xenograft-derived cells were treated like in (B) and limiting dilution assay was performed. The data were analyzed using ELDA software (red, 1.4A12 high; black, 1.4A12 low; the analyses are shown in Figure S2C).

(F) In vivo luciferase activity detected 90 days post-intracranial transplantation of 2,500 xenograft-derived LUC-positive GSC23c cells. The tumors were dissociated, and cells were acutely sorted for mAb 1.4A12 positivity before implantation into the mice.

(G) Statistic analysis of orthotopic tumor growth of sorted GSC23c cells with n = 5 and 6 mice/group as measured by luciferase activity over time (**$p < 0.01$, Mann-Whitney U test).

(H) Survival of mice engrafted with xenograft-derived GSC1 cells sorted for high and low expression of the mAb 1.4A12 antigen (**$p < 0.01$, log rank test; n = 7 mice/group).

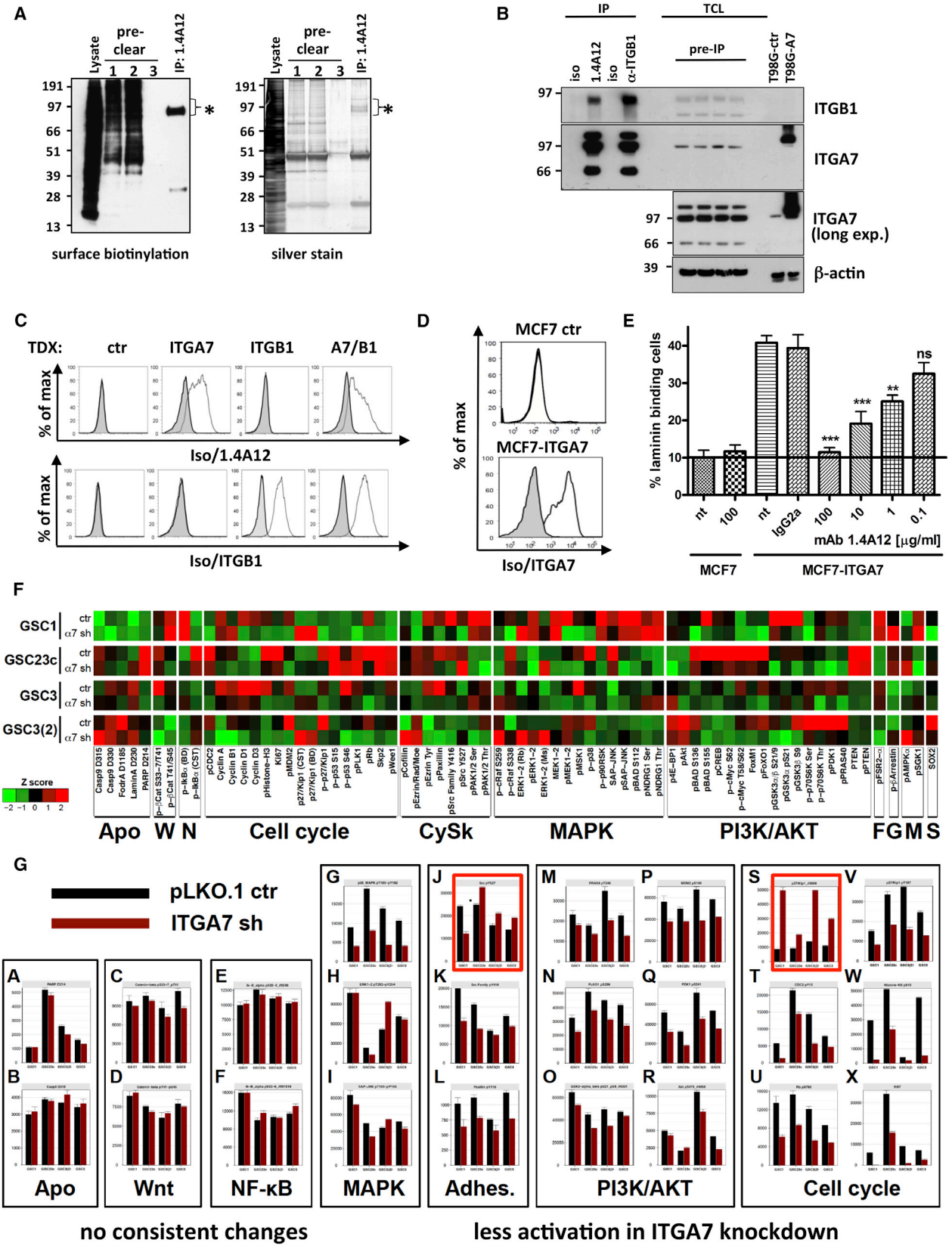

(legend on next page)

treated with ITGA7 shRNA, a strong upregulation of the cell cycle inhibitor p27/Kip1 as well as a decreased expression of S-phase kinase-associated protein 2 (Skp2), polo-like kinase (PLK), and Cyclin B1 (CycB) was observed (Figure 4D). ITGB1 KD led to the same phenotype (Figure 4E). This ruled out off-target effects of the shRNA and further underlined the importance of the ITGA7β1 dimer for cell cycle progression in GSCs. Consequently, in ITGA7-KD cells, the proliferation marker Ki67 was reduced, and cell cycle analysis showed an accumulation of nuclei in G0/1 phase, but no apoptotic nuclei with sub-diploid DNA content (Figure 4F).

Because also the activity of caspase 3/7 was not significantly elevated in ITGA7 or ITGB1 KD cells (Figures S4C and S4D), and the RPPA did not detect an increase of apoptosis-related endpoints, our data suggested that genetic neutralization of the ITGA7β1 dimer blocked the cell cycle without inducing apoptosis. These molecular events are in line with the significant growth decline of cells with reduced ITGA7 and ITGB1 expression (Figures 4G and S4E). Likewise, we observed a striking reduction in the clonogenic survival of cells treated with ITGA7 or ITGB1 shRNA by limiting dilution analysis (Figures 4H and S4F). Also pharmacological inhibition of AKT activity interfered with cell growth, which was not the case for p38 inhibition, indicating that the alteration in PI3K/AKT pathway contributed to the growth inhibition observed in ITGA7-KD cells (Figures S4G and S4H). Having confirmed the anti-proliferative effect of neutralizing ITGA7 by shRNA in vitro, we asked whether we could transfer the system into mouse models. When ITGA7 expression was suppressed (Figure S4I), GSC1 generated detectable tumors significantly later, while cells transduced with the control construct contributed to the tumor growth as expected (Figures S4J and S4K). Also by knocking down ITGA7 in GSC83 cells, which express this protein at lower levels (Figure S4I), we detected a significantly reduced growth (Figures S4L–S4N). Mice injected intracranially with cells transduced with a control shRNA construct showed strong bioluminescence signal 3 months post-engraftment (Figure 4I), while mice engrafted with ITGA7-KD cells showed no or very slow tumor growth (Figure 4J), and they survived more than 300 days without displaying any sign of neurological disorder (Figure 4K). These results indicated an important role of ITGA7 in the tumorigenicity of GSCs, suggesting that ITGA7 may represent a potentially valuable target for anti-tumor therapy.

High ITGA7 Expression Correlates with Worse Outcome in Patients with Brain Tumors

After confirming a correlation of ITGA7 mRNA and protein expression (Figure S5A), we analyzed its expression via publicly available databases, and we found a significant trend for increased ITGA7 expression in higher malignant brain tumors (Figures 5A and S5B). Of note, ITGA7 expression in normal human neural progenitor cells (NHNPs) was considerably lower than in GSCs (Figure 5B). These data pointed toward a correlation of ITGA7 expression and the aggressiveness of the tumor. ITGA3 and A6 belong to the same laminin-binding integrin subfamily as ITGA7, and they were described to play crucial roles in brain tumors. Therefore, we analyzed public databases also for their expression in glioma. The Repository for Molecular Brain Neoplasia Data (REMBRANDT) dataset for deceased glioma patients (Madhavan et al., 2009) revealed a significant better overall survival probability when tumors expressed lower levels of integrins. Compared to ITGA3 (Figure 5C) and ITGA6 (Figure 5D), the median survival of patients stratified for low ITGA7 expression (Figure 5E) was almost doubled. We further analyzed the expression distribution of tumors with high integrin levels. We found that the majority of patients with high ITGA3 and ITGA6 (85%) also expressed high levels of ITGA7 (Figure 5F). Interestingly, patients showing a co-expression of the three integrins had only a slightly worse outcome when compared to patients overexpressing only ITGA7 (Figure 5G). These data indicated that high expression of ITGA7 could represent a robust correlation marker with brain tumor malignancy.

In the most comprehensive low-grade glioma (LGG) expression dataset (The Cancer Genome Atlas [TCGA]), a clear population of patients overexpressed ITGA7 (Figure 5H). These had a median survival time of less than one-third compared to the patients with lower ITGA7 levels (Figure 5I). Also in LGG, ITGA7 expression had the strongest correlation with patient outcome when compared to the other two integrins (Figures S5C and S5D). Although ITGA7 levels were particularly elevated in high-grade glioma, patients with tumors expressing relatively lower

Figure 3. ITGA7 Is the Antigen of mAb 1.4A12

(A) Analysis of antigen bound by 1.4A12. Left: lysates of surface biotinylated GSC1 were immunoprecipitated with IgG2a control (preclears) or the 1.4A12 mAb. Associated proteins were detected with streptavidin-horseradish peroxidase (HRP). Right: silver staining of SDS-PAGE after immunoprecipitation is shown; in Figure S3A and Table S1, the Coomassie staining and identified proteins are shown. The brackets show the potential 1.4A12 antigen(s).

(B) Immunoprecipitation using control (iso), 1.4A12, or integin beta 1 mAb. Shown is the western blot analysis with the antibodies indicated. Vector- (ctr) and ITGA7-transduced T98G cells serve as specificity controls.

(C) Flow cytometric analysis of murine L929 cells transduced with GFP (ctr), ITGA7, ITGB1 alone, or in combination. Isotype control is shown as gray filled, and the antibody binding is shown as an open histogram.

(D) Flow cytometric analyses of mAb 1.4A12 on MCF7 wild-type (ctr) and ITGA7-overexpressing cells.

(E) Laminin adhesion assay: the indicated cells were plated on laminin-coated plastic for 45 min. After washing, the adhered cells were quantified in relation to the seeded cells. Shown are the average and SEM of three experiments (**$p < 0.01$ and ***$p < 0.001$, Student's t test versus IgG2a).

(F) Heatmap for 73 different (phospho-) proteins analyzed by reverse-phase protein array (RPPA). The cells were transduced with ITGA7-sh-containing lentiviral particles, and 8 days post-infection RPPA was performed. The heatmap shows the intensity of the signal obtained for the single proteins as compared to the average signal (signaling pathways were as follows: Apo, Apoptosis; W, Wnt; N, NF-κB; CySk, Cytoskeleton; F, FGFR; G, GPCR; M, mTOR; and S, Sox2).

(G) Summary of the effects of ITGA7 KD on the signaling pathways indicated. The bar plots shown in red frames indicate negative regulators of the pathways indicated. A, PARP(D214); B, Casp9(D315); C, b-cat(S33/T43); D, b-cat(T41/S45); E, IkBa(S32,CST); F, IkBa(S32,ABCAM); G, p38(T180/Y182); H, ERK1/2(T202/Y204); I, JNK(T183/Y185); J, Src(Y527); K, Src(Y416); L, Paxillin(Y118); M, PPRAS40(T246); N, FoxO1(S256); O, GSK3a/b(S9/S21); P, MDM2(S166); Q, PDK1(S241); R, AKT(S471); S, p27/Kip1; T, CDC2(Y15); U, pRB(S780); V, p27(T187); W, HH3(S10); X: Ki67.

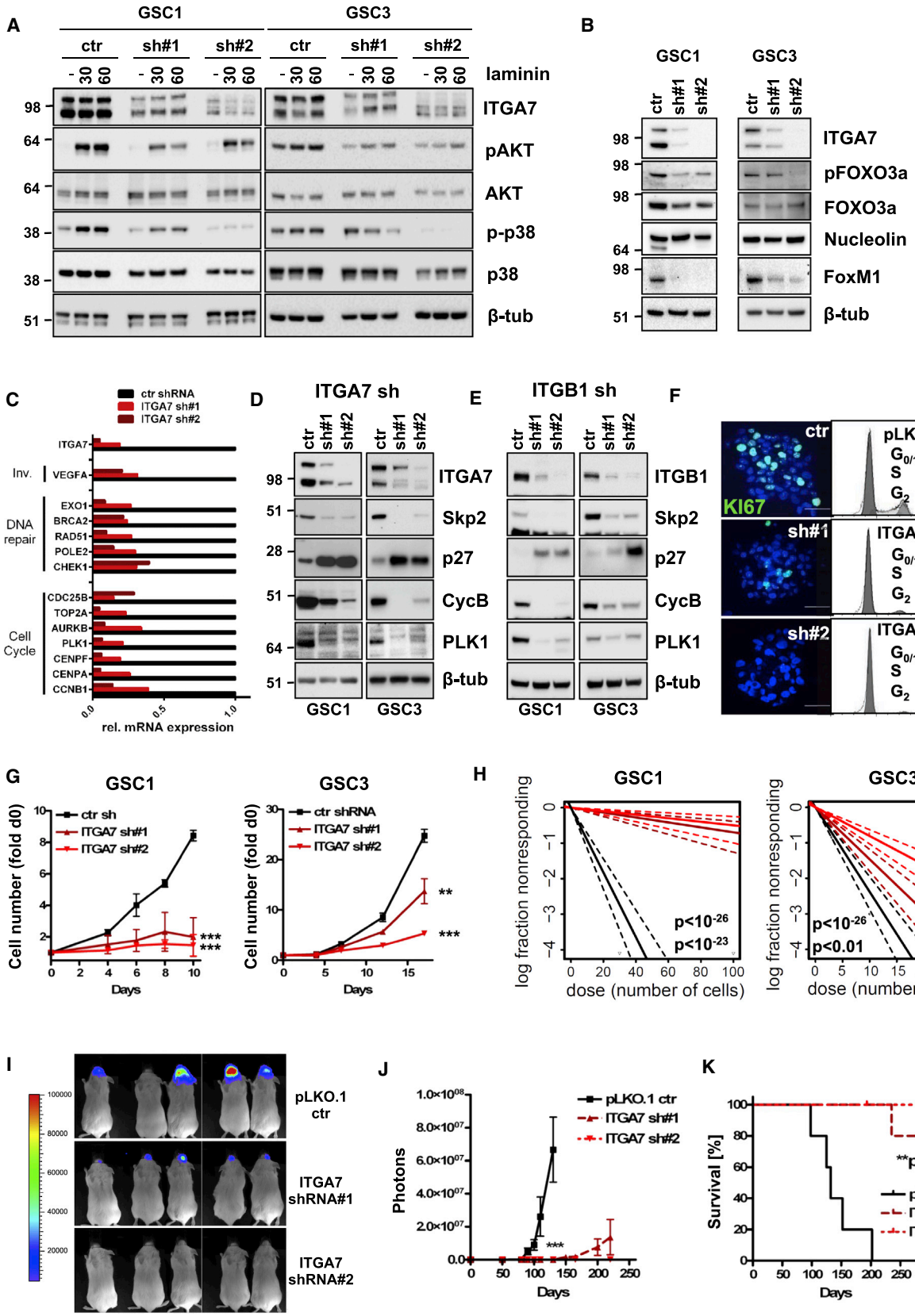

(legend on next page)

levels of ITGA7 had a significant survival advantage, even within the GBM datasets from TCGA (Brennan et al., 2013) and three other extensive gene expression profiling studies, while the GBM patients of the REMBRANDT dataset showed a strong trend (Figure 5J). Interestingly, the TCGA study indicated an elevated ITGA7 expression in GBM with mesenchymal and classical gene expression signature and a significantly lower but heterogeneous expression in the proneural subtype (Figures S5E and S5F). This resulted in a particularly low ITGA7 expression in a subset of patients from the proneural subtype, who showed a significant survival advantage (Figure S5G). In contrast, ITGA6 expression did not significantly correlate with patient outcome in any GBM subtype (Figure S5G). Taken together, these data indicate that glioma patients with low ITGA7 expression have better survival probabilities.

ITGA7 KD and Function-Blocking Antibody Impede Laminin Signaling and Invasion of GBM Cells In Vitro

It is well established that the ITGA7/β1 dimer binds and co-localizes with laminin in muscle cells (von der Mark et al., 2002) and mediates muscle cell migration (Yao et al., 1996). We detected a similar co-expression in both GBM neurospheres and tissue by immunofluorescence microscopy (Figures 6A and 6B). Further we found that GSCs lacking ITGA7 spread much less in matrigel when compared with control cells (Figure S6A). In quantitative laminin invasion assays, we detected a massive reduction of invasion upon KD of ITGA7 (Figure 6C), without a significant reduction in cell number in the time frame of the assay (Figure 6D), suggesting that ITGA7 is a critical mediator of cell spread and invasion of GSCs. Next, we investigated the intracellular pathways involved in integrin signaling. Upon cell seeding on laminin-coated plates, focal adhesion kinase (FAK) and Src were readily phosphorylated at Tyr397 and Tyr416, respectively (Figure S6B). This effect was blunted in ITGA7-KD cells (Figures 6E and S6C), confirming the role for ITGA7 in laminin-induced signaling in GSCs. Interestingly, the ablation of ITGA7 protein not only blocked the activation by exogenous laminin but also strongly reduced constitutive FAK and Src phosphorylation (Figure 6E), which might be induced by the endogenous laminin in the spheres. Taken together, these data suggested that ITGA7 is crucial for proper signaling induced by laminin in GSCs, and they can explain the ablation of the invasive capacity observed in cells knocked down for ITGA7.

By quantifying the number of integrin molecules on the cell surface of 13 independent primary GSC cultures, we found that the ITGA7 expression was more robust than ITGA6 and less heterogeneous than ITGA3 (Figures 6F, S6D, and S6E). Interestingly, cells expressing high levels of ITGA7 showed a tendency to express low levels of ITGA6 and vice versa (Figure 6F). Then, we investigated whether the KD of ITGB1 would also interfere with GSC invasion, and we detected a strongly reduced number of GSCs invading the laminin matrix, especially in cells with a complete depletion of ITGB1 (Figures S6F and S6G). The reduced invasiveness in ITGA7-KD cells might be partially attributable to the reduced p38 activity in the KD cells, as SB203580, a widely applied p38 inhibitor, significantly inhibited GSC invasion, while AKT inhibitors did not (Figure S6H). Of note, anti-ITGA7 reduced GSC spreading into the matrigel matrix (Figure S6I), while invasion assays revealed a strong, concentration-dependent inhibition of laminin invasion by the intact antibody and the F(ab) fragments generated from anti-ITGA7 in GSCs (Figures 6G, S6J, and S6K). As expected, the blocking of ITGB1 was even more effective due to the inhibition of all β1-containing integrin dimers. Interestingly, antibodies blocking ITGA3 and ITGA6 (Lathia et al., 2010) significantly inhibited migration only in GSCs expressing low ITGA7 levels (Figures 6F–6H). The treatment of cells with anti-ITGA7 had only a marginal impact on p-p38 levels, but it induced a massive reduction in laminin-induced FAK and Src phosphorylation (Figures 6I and S6L), suggesting that laminin invasion is primarily mediated by these signaling mediators.

Antibody-mediated inhibition of cell invasion was also observed in vivo. Mice were intracranially injected with GFP-expressing GSCs, and they were treated with 10 mg/kg antibody (intraperitoneally [i.p.]) twice weekly starting 14 days post-engraftment, while the blood-brain barrier (BBB) was still disrupted due to the cell implantation (data not shown). After 60 days the invasion depth of GFP-positive cells into the normal tissue showed a significant reduction in mice treated with anti-ITGA7 antibody (Figures 6J and 6K). These results highlight that ITGA7 plays a major role in GSC invasion and laminin-induced

Figure 4. Inhibition of ITGA7 by shRNA Impairs Growth of Primary GBM Cells In Vitro and In Vivo

(A) Western blot analysis of GSC1 and GSC3 cells transduced with either control shRNA or two independent ITGA7-targeting shRNAs and plated on laminin-coated plastic for the time and with the antibodies indicated (see also Figure S4).

(B) Cells were transduced as in (A) and western blot analysis for the proteins indicated was performed 8 days post-transduction.

(C) Analysis for the mRNA expression of FoxM1 target genes with major functions in the regulation of cell cycle, DNA repair, and invasion upon ITGA7 KD (shown are the results of a representative qPCR; mRNA expression was normalized to the cells infected with pLKO.1 ctr).

(D) Western blot analysis of GSC1 and GSC3 cells transduced with control shRNA or two independent ITGA7-targeting shRNAs.

(E) Western blot analysis of GSC1 and GSC3 cells transduced with control shRNA or two independent ITGA6-targeting shRNAs. For (D) and (E), the membranes were probed with the antibodies recognizing the proteins indicated.

(F) Representative Ki67 immunofluorescence and cell cycle analyses of GSC1 spheres knocked down for ITGA7 (sh#1 and sh#2). Representative histograms obtained by flow cytometry are shown (scale bar, 40 μm).

(G) GSC1 and GSC3 cells were transduced with a control vector (ctr-shRNA) or for shRNA targeting ITGA7 expression. Cell numbers were compared to day 0 and the fold increase was plotted. Shown are the average and SEM of three independent experiments (**$p < 0.01$ and ***$p < 0.001$, ANOVA).

(H) For the limiting dilution assay, GSC1 and GSC3 cells were treated as in (F). Shown are the log/dose slopes and p values calculated by ELDA analysis (black, ctr shRNA; dark red, ITGA7 shRNA#1; and light red, ITGA7 shRNA#2). Similar results were obtained for ITGB1 KD. See also Figures S4E and S4F.

(I) In vivo luciferase activity detected 90 days post-intracranial transplantation of 5×10^4 GSC1 cells transduced with the shRNA constructs indicated.

(J) Statistic analysis of orthotopic tumor growth with n = 5 mice/group as measured by luciferase activity over time (***$p < 0.001$, ANOVA).

(K) Survival analysis of mice described in (H) (n = 5 mice/group; **$p < 0.005$, log rank test).

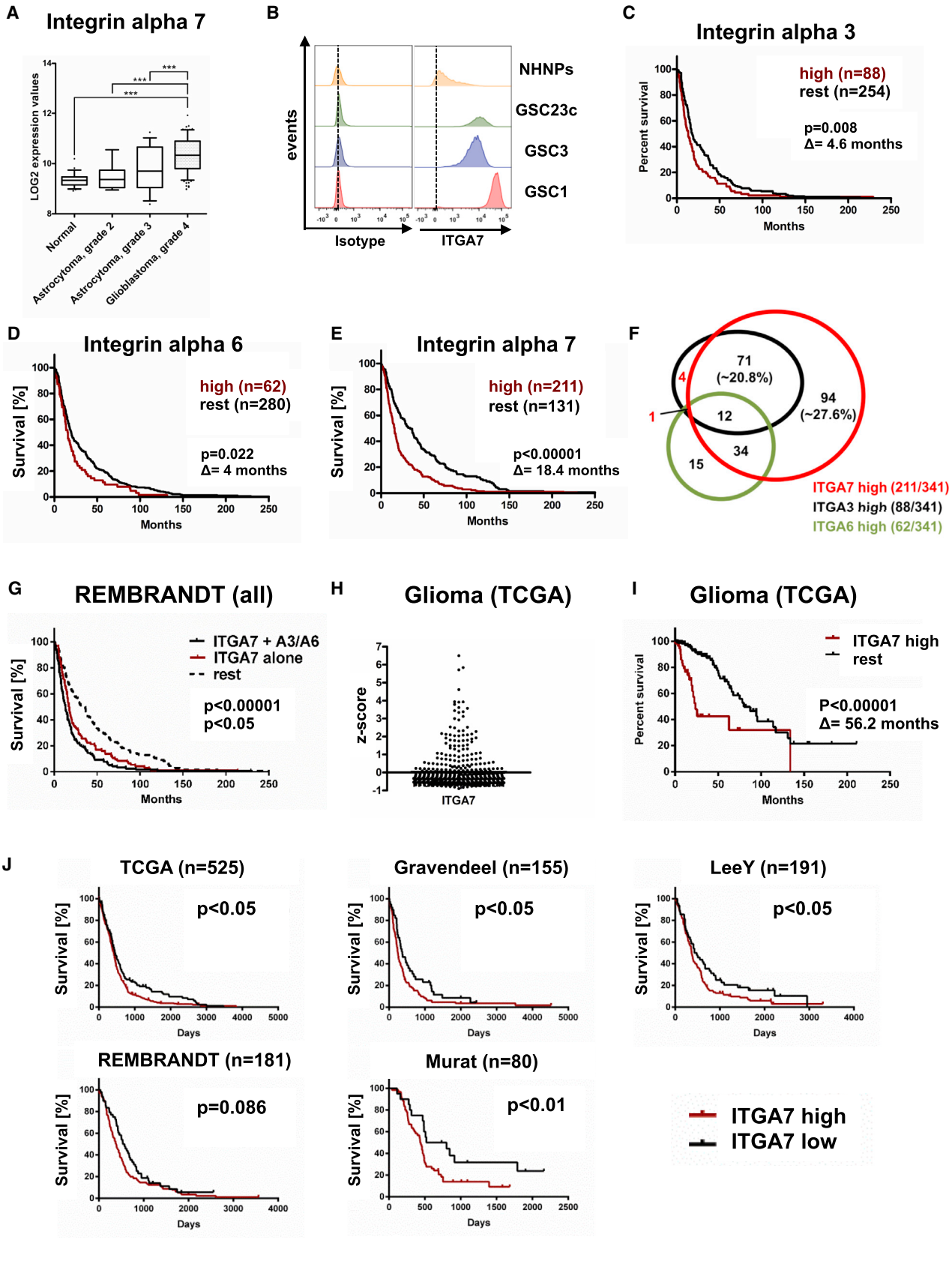

(legend on next page)

outside-in signaling, which can be blocked by the anti-ITGA7 antibody generated in this study.

Anti-ITGA7 Antibody Suppresses Tumor Growth and Invasion In Vivo

We noted that a significant fraction of GBM patients and GSC cultures (Figures 5F and 6F) expressed high levels of ITGA7 as primary laminin-binding integrin. To test a potential therapeutic activity of our mAb in this subset of GBM, we subcutaneously injected two independent luciferase-expressing GSC cultures expressing high and intermediate levels of ITGA7 (GSC1 and GSC3), and we treated the mice with two weekly doses of 10 mg/kg anti-ITGA7 or isotype-matched control mAb. While the luciferase activity was equal 5 days after implantation (Figures 7A and S7A), at later time points, the tumor growth was significantly impaired in the mice treated with anti-ITGA7 (Figures 7B, S7B, and S7C). Although the tumors in treated mice started to grow 30 days after discontinuation of antibody injections, a reduction in size was still evident more than 4 months after the last treatment (Figures 7C and S7D). The tumors in the mice treated with anti-ITGA7 showed significantly less Ki67-positive cells compared to the control (Figure 7D). Also, the activation status of FAK and AKT appeared to be reduced when analyzed by western blot and immunofluorescence analyses in the mAb-treated subcutaneous xenografts (Figures S7E–S7H).

To extend these data, we used intracranial brain xenografts of GSCs, which closely mimic the behavior of malignant glioma. In the presence of 3 μg anti-ITGA7 or isotype control (IgG2a), the cells were grafted in the striatum of mice. Taking into account that the BBB requires around 3–4 weeks to repair after mechanical damage of implantation, mice were treated twice weekly with 10 mg/kg antibody by systemic injection for 4 weeks. We observed significantly longer survival times in anti-ITGA7-treated mice as compared to the control animals (Figure 7E). To investigate the anti-tumor activity of our antibody in more detail, we repeated the experiment with GFP-expressing GSC1 and analyzed the brains histologically. Eight weeks after grafting, control mice harbored tumors that invaded the homolateral striatum, piriform cortex, corpus callosum, anterior commissure, internal capsule, optic tract, septal nuclei, and fimbria-hippocampus, whereas very limited brain invasion was detected in anti-ITGA7-treated mice (Figure 7F). Treatment with anti-ITGA7 dramatically lowered the number of tumor cells that infiltrated the corpus callosum (CC), which scored 8.75 ± 2.02 cells (mean ± SEM) and 80.25 ± 8.49 cells in anti-ITGA7-treated mice and controls, respectively ($p < 0.001$; Figure 7G). The number of cells in the anterior commissure (AC) was also significantly lower in anti-ITGA7-treated animals compared to controls (143.5 + 18.12 cells and 17.75 + 4.31 cells, respectively; $p < 0.001$). The volume of the brain region invaded by GFP+ cells was 4.22 ± 0.71 mm^3 (mean ± SEM) and 11.02 ± 1.29 mm^3 in anti-ITGA7-treated mice and in control mice, respectively ($p < 0.005$; Figure 7H). At the brain site where anti-ITGA7 was injected, we did not observe any pathological changes of the brain parenchyma, suggesting the absence of inflammation or toxicity. Twelve weeks after grafting, the tumor volume dramatically increased in both groups. However, while the tumor cells in the control mice strongly infiltrated the contralateral cerebral hemisphere, cell spreading was still significantly reduced in brains of anti-ITGA7-treated mice even 8 weeks after ceasing treatment (Figure 7F).

DISCUSSION

Using an unbiased antibody-mediated screening for surface proteins abundantly expressed in undifferentiated GSCs, we identified ITGA7 as a new biomarker and potential therapeutic target in GBM. Our data demonstrated that, while upregulated on the surface of primary tumorigenic GBM cells, ITGA7 expression is markedly reduced upon differentiation and weakly expressed in conventional GBM cell lines. This may explain why the role of ITGA7 in GBM has been neglected in the past. Although the main known physiological role of ITGA7 involves function and survival of mesenchymal tissues, such as skeletal and vascular smooth muscle (Flintoff-Dye et al., 2005; Hayashi et al., 1998; Mayer et al., 1997), ITGA7 was proposed as a tumor suppressor based on the reduced growth and invasion observed after ectopic expression in melanoma and prostate cancer models (Han et al., 2010; Ren et al., 2007; Zhu et al., 2010; Ziober et al., 1999).

In contrast to these studies based on exogenous overexpression on other tumor types, here we provide striking evidence for an opposite function of ITGA7 in GBM. We found that ITGA7 can

Figure 5. ITGA7 Expression in Brain Tumors Correlates with Worse Patient Outcome

(A) ITGA7 expression data from a study by Sun et al. (2006) (***$p < 0.001$, Mann-Whitney U test). The mRNA/protein correlation is shown in Figure S5A.

(B) Representative flow cytometric analyses for the ITGA7 surface expression on normal human neuronal progenitor cells (NHNPs) and three independent GSC lines.

(C) Clinical outcome of glioma patients in the REMBRANDT dataset is correlated with the expression level of ITGA3. High-expressing patients were defined as >2-fold of the median ITGA3 expression.

(D) Clinical outcome of glioma patients described in (C) correlated with the expression level of ITGA6.

(E) Clinical outcome of glioma patients described in (C) correlated with the expression level of ITGA7.

(F) Venn diagram illustrating the distribution of gliomas with high (>2-fold median) expression of ITGA3 (black), ITGA6 (green), and ITGA7 (red) (B–D).

(G) Clinical outcome of patients highly expressing ITGA7 alone or in combination with ITGA3 and/or ITGA6 versus patient with low ITGA7 expression (cutoff is >2-fold median expression).

(H) Distribution of ITGA7 expression of TCGA low-grade glioma dataset is plotted as the *Z* scores.

(I) Clinical outcome of low-grade glioma patients in the TCGA dataset is correlated with the expression level of ITGA7. High-expressing patients were defined as *Z* score > 0.

(J) Clinical outcomes of five comprehensive GBM patient datasets are correlated with the expression level of ITGA7. Patients groups were stratified by lower quartile (ITGA7 low) versus the remaining patients (ITGA7 high). Statistics for all Kaplan-Meier plot (KM) analyses were performed using log rank test.

See also Figure S5.

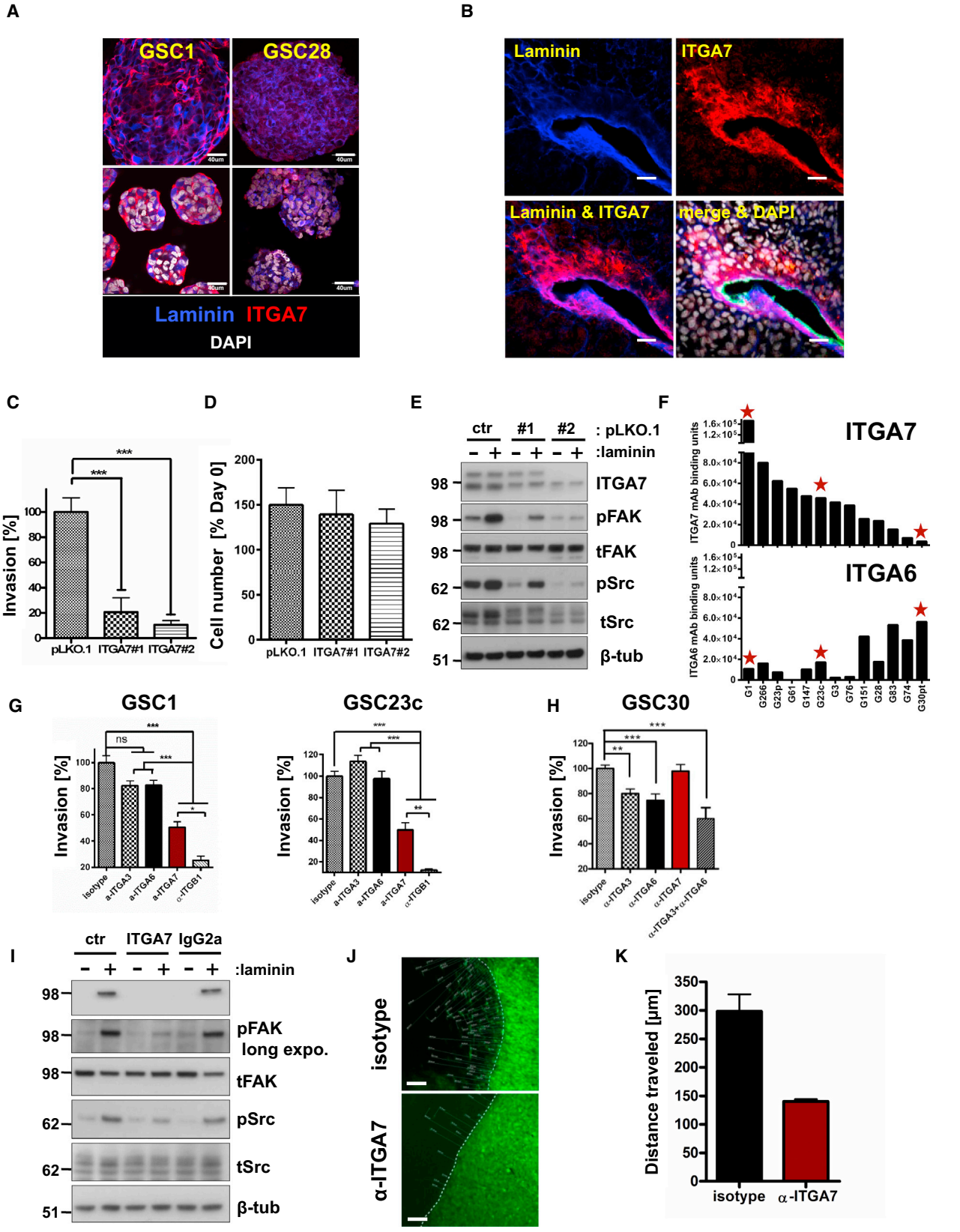

(legend on next page)

serve as a GSC marker. In GSC xenografts and primary GBM specimens, ITGA7 is enriched in the perivascular niche and co-localizes with its ligand laminin. Functional studies revealed an essential role of ITGA7 in two of the most critical GBM traits, aberrant cell proliferation and invasion. GSC fate depends on ITGA7 signaling; in fact, gene silencing almost abolished GSC proliferation in vitro and in vivo. Our results are in line with recent findings on esophageal carcinoma, where ITGA7 may serve as a functional cancer stem cell marker (Ming et al., 2016). We found that functional neutralization of ITGA7, either by shRNA or antibody, strongly inhibited laminin-induced FAK, AKT, and Src activation, which are major mediators of extracellular matrix (ECM)-induced proliferation signals and may serve as potential targets for therapy (D'Abaco and Kaye, 2008; Kim et al., 2009). In GSCs deficient for ITGA7, we observed a loss of cellular FoxM1, a critical regulator of stemness, invasion, and cell cycle progression (Gemenetzidis et al., 2010; Wang et al., 2011). These data could be explained by the decreased AKT activity (Brunet et al., 1999), which was shown to regulate the expression of FoxM1 by inhibiting FOXO3a functions (Karadedou et al., 2012). We also observed a reduction of the ubiquitin ligase Skp2, which is normally stabilized by attachment signals and mediates the degradation of the cell cycle inhibitor p27/KIP1 that is elevated in ITGA7 KD cells (Bond et al., 2004; Carrano and Pagano, 2001).

In summary, our data demonstrate a central role of ITGA7 for laminin-induced outside-in signaling (Legate et al., 2009) in GSC. This is in line with the observation that ITGA7 interacts with laminin 2 (Yao et al., 1996), which is aberrantly expressed in GBM (Lathia et al., 2012). Selection of both ITGA6 and ITGA7 bright cells enriches for highly clonogenic tumor-initiating cells in GBM. However, although a high degree of sequence homology (>60%) and similar substrate specificities exist, we found that ITGA7 is more abundant than ITGA6 in GSCs and distinguishes patients outcome in glioma better when compared to the other ITGB1 partners for laminin binding.

Taking advantage of the GlioVis database, the analyses of five independent large-scale gene expression datasets (Bowman et al., 2017) showed an aberrant high ITGA7 mRNA expression in GBM. Most of GBM patients with lower ITGA7 levels belonged to the proneural subtype and showed a considerably better survival. Moreover, in both TCGA LGG and REMBRANDT datasets, high ITGA7 expression correlated robustly with worse patient outcome, significantly more than the two other major laminin-binding integrins ITGA3 and ITGA6 (Lathia et al., 2010; Nakada et al., 2013). Analysis of integrin surface expression indicated that a large subset of GSCs expressed primarily ITGA7 as laminin receptor. Interestingly, the same was true when tumors from patients of the REMBRANDT dataset were grouped for high integrin expression. This analysis showed a considerable superiority of ITGA7 on both ITGA3 and ITGA6 in terms of expression and correlation with patient outcome. Although the different contribution of laminin-binding integrins in single GBMs remains to be evaluated in more detail, our data provide strong evidence for a key role played by ITGA7 as the major laminin receptor promoting tumor growth and spreading.

Activation of FAK and Src by ECM is required to trigger tumor cell invasion, which is a key mechanism responsible for the detrimental prognosis of GBM patients (Dunn et al., 2012) and a potential target for therapeutic intervention (Desgrosellier and Cheresh, 2010; Kleber et al., 2008; Zhong et al., 2010). We have shown that inhibition of ITGA7 functions by using either gene silencing or antibodies strongly reduced the invasion of GSCs in vitro and in vivo. The engraftment and outgrowth of the tumor cells in immunodeficient mice was considerably delayed when ITGA7 function was neutralized by shRNA or blocking mAb. To our knowledge, currently there are no ITGA7 inhibitors under development. Because BBB is a major limitation for the antibody penetrance to the brain, we treated mice systemically with anti-ITGA7 for only 4 weeks after the BBB impairment caused by needle implantation, which requires at least 3–4 weeks for complete recovery. Our findings could be theoretically translated into the clinics by treating GBM patients with anti-ITGA7 after the BBB disruption that follows brain surgery. Although the goal of this therapy would be mainly to slow down tumor recurrence and infiltration, the finding that ITGA7 is a key player in GSC proliferation and migration may foster the development of new strategies and therapeutic opportunities based on ITGA7 targeting.

Figure 6. ITGA7 Is Co-expressed with Laminin in GBM and Mediates Laminin-Induced Signaling and Invasion

(A) Immunofluorescence picture of spheres from two different GSCs stained with the antibodies indicated.

(B) Immunofluorescence picture of a frozen primary GBM patient tumor specimen stained with the antibodies indicated (for A and B, scale bars represent 40 μm).

(C) Invasion of GSC1 in transwell chambers coated with laminin. After 48 hr, the invasion of cells transduced with the shRNA constructs indicated was quantified. Shown are the average and SEM of three independent experiments done in triplicate (***$p < 0.001$, ANOVA).

(D) Change of cell numbers as determined by ATP content in the time frame of the invasion assay described in (C).

(E) GSC1 cells treated with ctr or ITGA7 shRNA containing lentiviral particles were incubated in laminin-coated plates for 30 min, cells were lysed, and western blot analysis was performed for the proteins indicated.

(F) Quantification of ITGA6 and ITGA7 surface expression of GSC panel as antibody-binding units as determined by QIFIKIT (see also Figures S6D and S6E). The stars indicate GSCs tested for invasion.

(G) Invasion of GSCs with different alpha integrin expression in transwell chambers coated with laminin. After 48 hr in the presence of the antibodies indicated (10 μg/mL), the invaded cells were stained with Calcein AM and analyzed with ImageJ, as described in the STAR Methods. Shown are the average and SEM of three independent experiments done in triplicate (***$p < 0.001$ and **$p < 0.01$, ANOVA).

(H) Invasion assay with GSCs expressing low ITGA7 levels (GSC30, ***$p < 0.001$; **$p < 0.01$; ANOVA).

(I) GSC1 cells were preincubated with anti-ITGA7 (1.4A12), isotype control antibody, or PBS (ctr) for 15 min at 37°C, then seeded on laminin-coated plates for 30 min and lysed. Western blot analysis for the indicated proteins was performed.

(J) Mice were intracranially injected with GFP-expressing GSC1. Then 12 days post-inoculation, treatment twice weekly with 10 mg/kg α-ITGA7 antibody (1.4A12) or isotype control mAb started. After 60 days of continuous treatment the brains were removed. The traveling distances of cells invading the caudal portion of the striatum were analyzed. Shown is a representative immunofluorescence (IF) picture (scale bar, 200 μm).

(K) Statistic analysis of the invasion depth of the tumors cells described in (I) (n = 3 mouse brains/treatment).

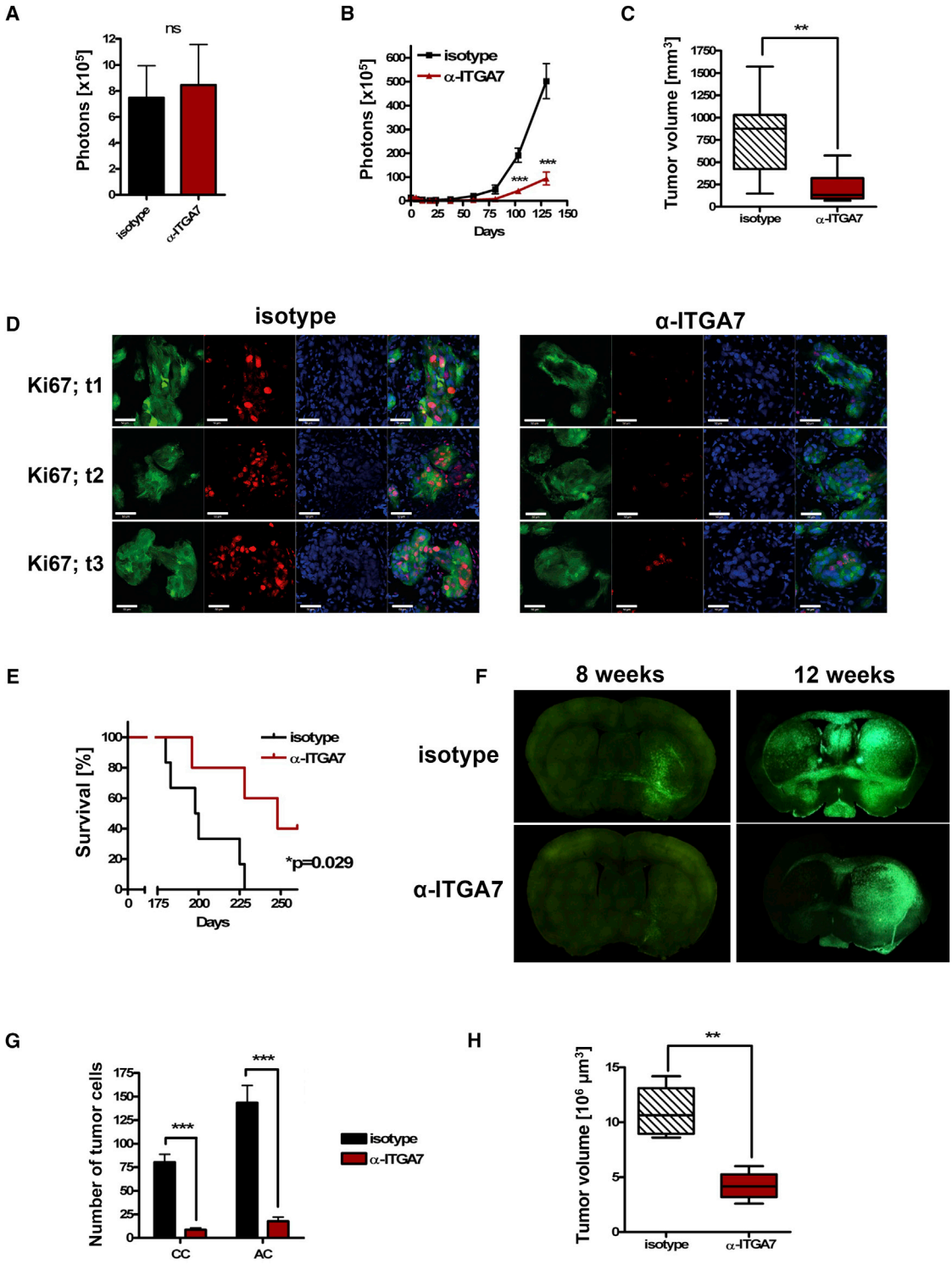

Figure 7. α-ITGA7 Impairs GBM Tumor Growth and Invasion In Vivo

(A) Luciferase activity detected with a Xenogen IVIS 100 small animal in vivo imaging system, 5 days post-sc transplantation of 5 X 10^5 GSC1-LUC cells in mice either treated with anti-ITGA7 (α-ITGA7) antibody or isotype control (i.p.).

(B) Analysis of sc GSC1-LUC tumor growth over time in mice treated either with isotype control or with α-ITGA7 antibody (1.4A12). Shown is the average photon count and SEM of n = 6 mice/group measured by Xenogen IVIS 100 small animal in vivo imaging system (***$p < 0.001$, two-tailed Student's t test). See also Figure S7.

(C) Analyses of the tumor volumes 5 months after ceasing the anti-ITGA7 treatment. Shown is the size of the sc tumors of n = 6 mice/group measured by calliper (**$p < 0.01$, two-tailed Student's t test).

(legend continued on next page)

STAR★METHODS

Detailed methods are provided in the online version of this paper and include the following:

- KEY RESOURCES TABLE
- CONTACT FOR REAGENT AND RESOURCES SHARING
- ANIMAL STUDIES
  - Mouse strains used
  - Detailed description of the mouse models
  - Cell Lines
- METHOD DETAILS
  - Hybridoma generation
  - High throughput hybridoma screening
  - Microarray Database Analyses
  - Immunoprecipitation
  - Mass spectrometry
  - Lentiviral constructs
  - Whole brain reconstructions and tumor cells invasion analysis
  - Immunofluorescence Microscopy
  - Real-Time PCR
  - Western Blotting
  - Flow Cytometric Analysis
  - Tissue Processing and Cell Sorting
  - Cell Cycle Analysis
  - Cell Viability and Caspase 3/7 Assay
  - Limiting Dilution Assay
  - Invasion Assay
  - Reverse Phase Protein Microarrays
- QUANTIFICATION AND STATISTICAL ANALYSIS DATA
- DATA AND SOFTWARE AVAILABILITY

SUPPLEMENTAL INFORMATION

Supplemental Information includes seven figures and three tables and can be found with this article online at http://dx.doi.org/10.1016/j.stem.2017.04.009.

AUTHOR CONTRIBUTIONS

Conceptualization, T.L.H. and R.D.M.; Methodology, T.L.H.; Investigation, T.L.H., M.R.S., L.B., C.V., M. Signore, M.E.F., S.d.M., U.W., M.P., S.G., A.B., C.D.S., and L.M.; Software, A.C. and M. Signore; Writing – Original Draft, T.L.H. and R.D.M.; Writing – Review & Editing, T.L.H. and R.D.M.; Funding Acquisition, R.D.M.; Resources, L.R.-V., R.P., M.B., and M. Schnölzer; Supervision, T.L.H., R.P., and R.D.M.

ACKNOWLEDGMENTS

We thank Luca Pasquini, Eleonora Petrucci, Mario Falchi, and Federica Ganci for support performing experiments. We thank Rosanna Dattilo, Paola Di Matteo Gabriele De Luca, Massimo Spada, and Marta Baiocchi for help with in vitro and in vivo CSC culture. We thank Desiree Bonci and Simone Fulda for vectors and cell lines. We thank Valeria Coppola and Giuseppe Loreto for help in preparing the manuscript. This work was supported by the FIRB grant (RBAP10KJC5_004) by the Italian Ministry of University and Research, the Ministero della Salute (RF-2011-02349985), and the Italian Association for Cancer Research (AIRC; IG 2013 N.14574 to R.P.). T.L.H. was supported by the EU Marie Curie Research Training Network "ApopTrain" (MRTN-CT-2006-035624).

Received: July 6, 2016
Revised: February 16, 2017
Accepted: April 20, 2017
Published: June 8, 2017

REFERENCES

Binda, E., Visioli, A., Giani, F., Lamorte, G., Copetti, M., Pitter, K.L., Huse, J.T., Cajola, L., Zanetti, N., DiMeco, F., et al. (2012). The EphA2 receptor drives self-renewal and tumorigenicity in stem-like tumor-propagating cells from human glioblastomas. Cancer Cell *22*, 765–780.

Bonci, D., Cittadini, A., Latronico, M.V., Borello, U., Aycock, J.K., Drusco, A., Innocenzi, A., Follenzi, A., Lavitrano, M., Monti, M.G., et al. (2003). 'Advanced' generation lentiviruses as efficient vectors for cardiomyocyte gene transduction in vitro and in vivo. Gene Ther. *10*, 630–636.

Bond, M., Sala-Newby, G.B., and Newby, A.C. (2004). Focal adhesion kinase (FAK)-dependent regulation of S-phase kinase-associated protein-2 (Skp-2) stability. A novel mechanism regulating smooth muscle cell proliferation. J. Biol. Chem. *279*, 37304–37310.

Bowman, R.L., Wang, Q., Carro, A., Verhaak, R.G., and Squatrito, M. (2017). GlioVis data portal for visualization and analysis of brain tumor expression datasets. Neuro-oncol. *19*, 139–141.

Brennan, C.W., Verhaak, R.G., McKenna, A., Campos, B., Noushmehr, H., Salama, S.R., Zheng, S., Chakravarty, D., Sanborn, J.Z., Berman, S.H., et al.; TCGA Research Network (2013). The somatic genomic landscape of glioblastoma. Cell *155*, 462–477.

Brunet, A., Bonni, A., Zigmond, M.J., Lin, M.Z., Juo, P., Hu, L.S., Anderson, M.J., Arden, K.C., Blenis, J., and Greenberg, M.E. (1999). Akt promotes cell survival by phosphorylating and inhibiting a Forkhead transcription factor. Cell *96*, 857–868.

Carrano, A.C., and Pagano, M. (2001). Role of the F-box protein Skp2 in adhesion-dependent cell cycle progression. J. Cell Biol. *153*, 1381–1390.

Cheng, L., Huang, Z., Zhou, W., Wu, Q., Donnola, S., Liu, J.K., Fang, X., Sloan, A.E., Mao, Y., Lathia, J.D., et al. (2013). Glioblastoma stem cells generate vascular pericytes to support vessel function and tumor growth. Cell *153*, 139–152.

D'Abaco, G.M., and Kaye, A.H. (2008). Integrin-linked kinase: a potential therapeutic target for the treatment of glioma. J. Clin. Neurosci. *15*, 1079–1084.

Day, B.W., Stringer, B.W., Al-Ejeh, F., Ting, M.J., Wilson, J., Ensbey, K.S., Jamieson, P.R., Bruce, Z.C., Lim, Y.C., Offenhäuser, C., et al. (2013). EphA3 maintains tumorigenicity and is a therapeutic target in glioblastoma multiforme. Cancer Cell *23*, 238–248.

(D) Analysis of cell proliferation in subcutaneous xenografts by immunofluorescence resulted in a decrease in Ki67/GFP double-positive tumor cells in anti-ITGA7- compared to isotype control-treated mice. Shown are representative pictures of three xenografts/treatment (24.87 ± 4.30 versus 47.72 ± 4.21, mean ± SEM; $p = 0.0089$, Student's t test). In Figures S7G and S7H, the phosphorylation status of FAK and AKT are shown.
(E) Survival of mice intracranially engrafted with 1×10^4 GSC1-LUC cells and treated either with isotype control or with anti-ITGA7 (α-ITGA7) antibody. The time until the mice showed a clear neurological sign is plotted. The experiment was terminated 260 days after orthotopic implantation (n = 5 and 6 mice/group; $^*p = 0.029$, log rank test).
(F) Representative pictures of a mouse brain slice showing the location of the GFP-positive tumor cells 8 weeks and 12 weeks after intracranial injection of 5×10^4 GSC1-GFP. The systemic mAb 1.4A12 treatment (α-ITGA7) was performed for 4 weeks, twice a week.
(G) Number of tumor cells that infiltrated the corpus callosum (CC) and the anterior commissure (AC) 8 weeks after engraftment. Shown is the average and SEM of four mouse brains ($^{***}p < 0.001$, Student's t test).
(H) Statistic analysis of the tumor volumes 8 weeks after injection. Shown is a boxplot of four mouse brains ($^{**}p < 0.005$, Student's t test).

Desgrosellier, J.S., and Cheresh, D.A. (2010). Integrins in cancer: biological implications and therapeutic opportunities. Nat. Rev. Cancer *10*, 9–22.

Dunn, G.P., Rinne, M.L., Wykosky, J., Genovese, G., Quayle, S.N., Dunn, I.F., Agarwalla, P.K., Chheda, M.G., Campos, B., Wang, A., et al. (2012). Emerging insights into the molecular and cellular basis of glioblastoma. Genes Dev. *26*, 756–784.

Flintoff-Dye, N.L., Welser, J., Rooney, J., Scowen, P., Tamowski, S., Hatton, W., and Burkin, D.J. (2005). Role for the alpha7beta1 integrin in vascular development and integrity. Dev. Dyn. *234*, 11–21.

Galli, R., Binda, E., Orfanelli, U., Cipelletti, B., Gritti, A., De Vitis, S., Fiocco, R., Foroni, C., Dimeco, F., and Vescovi, A. (2004). Isolation and characterization of tumorigenic, stem-like neural precursors from human glioblastoma. Cancer Res. *64*, 7011–7021.

Gemenetzidis, E., Elena-Costea, D., Parkinson, E.K., Waseem, A., Wan, H., and Teh, M.T. (2010). Induction of human epithelial stem/progenitor expansion by FOXM1. Cancer Res. *70*, 9515–9526.

Han, Y.C., Yu, Y.P., Nelson, J., Wu, C., Wang, H., Michalopoulos, G.K., and Luo, J.H. (2010). Interaction of integrin-linked kinase and miniature chromosome maintenance 7-mediating integrin alpha7 induced cell growth suppression. Cancer Res. *70*, 4375–4384.

Hayashi, Y.K., Chou, F.L., Engvall, E., Ogawa, M., Matsuda, C., Hirabayashi, S., Yokochi, K., Ziober, B.L., Kramer, R.H., Kaufman, S.J., et al. (1998). Mutations in the integrin alpha7 gene cause congenital myopathy. Nat. Genet. *19*, 94–97.

Hu, Y., and Smyth, G.K. (2009). ELDA: extreme limiting dilution analysis for comparing depleted and enriched populations in stem cell and other assays. J. Immunol. Methods *347*, 70–78.

Johnson, D.R., and O'Neill, B.P. (2012). Glioblastoma survival in the United States before and during the temozolomide era. J. Neurooncol. *107*, 359–364.

Karadedou, C.T., Gomes, A.R., Chen, J., Petkovic, M., Ho, K.K., Zwolinska, A.K., Feltes, A., Wong, S.Y., Chan, K.Y., Cheung, Y.N., et al. (2012). FOXO3a represses VEGF expression through FOXM1-dependent and -independent mechanisms in breast cancer. Oncogene *31*, 1845–1858.

Kim, L.C., Song, L., and Haura, E.B. (2009). Src kinases as therapeutic targets for cancer. Nat. Rev. Clin. Oncol. *6*, 587–595.

Kleber, S., Sancho-Martinez, I., Wiestler, B., Beisel, A., Gieffers, C., Hill, O., Thiemann, M., Mueller, W., Sykora, J., Kuhn, A., et al. (2008). Yes and PI3K bind CD95 to signal invasion of glioblastoma. Cancer Cell *13*, 235–248.

Lathia, J.D., Gallagher, J., Heddleston, J.M., Wang, J., Eyler, C.E., Macswords, J., Wu, Q., Vasanji, A., McLendon, R.E., Hjelmeland, A.B., and Rich, J.N. (2010). Integrin alpha 6 regulates glioblastoma stem cells. Cell Stem Cell *6*, 421–432.

Lathia, J.D., Li, M., Hall, P.E., Gallagher, J., Hale, J.S., Wu, Q., Venere, M., Levy, E., Rani, M.R., Huang, P., et al. (2012). Laminin alpha 2 enables glioblastoma stem cell growth. Ann. Neurol. *72*, 766–778.

Legate, K.R., Wickström, S.A., and Fässler, R. (2009). Genetic and cell biological analysis of integrin outside-in signaling. Genes Dev. *23*, 397–418.

Madhavan, S., Zenklusen, J.C., Kotliarov, Y., Sahni, H., Fine, H.A., and Buetow, K. (2009). Rembrandt: helping personalized medicine become a reality through integrative translational research. Mol. Cancer Res. *7*, 157–167.

Marziali, G., Signore, M., Buccarelli, M., Grande, S., Palma, A., Biffoni, M., Rosi, A., D'Alessandris, Q.G., Martini, M., Larocca, L.M., et al. (2016). Metabolic/Proteomic Signature Defines Two Glioblastoma Subtypes With Different Clinical Outcome. Sci. Rep. *6*, 21557.

Mayer, U., Saher, G., Fässler, R., Bornemann, A., Echtermeyer, F., von der Mark, H., Miosge, N., Pöschl, E., and von der Mark, K. (1997). Absence of integrin alpha 7 causes a novel form of muscular dystrophy. Nat. Genet. *17*, 318–323.

Ming, X., Fu, L., Zhang, L., Qin, Y., Cao, T., Chan, K., Ma, S., Xie, D., and Guan, X. (2016). *Integrin α7* is a functional cancer stem cell surface marker in oesophageal squamous cell carcinoma. Nat. Commun. *7*, 13568.

Nakada, M., Nambu, E., Furuyama, N., Yoshida, Y., Takino, T., Hayashi, Y., Sato, H., Sai, Y., Tsuji, T., Miyamoto, K.I., et al. (2013). Integrin α3 is overexpressed in glioma stem-like cells and promotes invasion. Br. J. Cancer *108*, 2516–2524.

Pollard, S.M., Yoshikawa, K., Clarke, I.D., Danovi, D., Stricker, S., Russell, R., Bayani, J., Head, R., Lee, M., Bernstein, M., et al. (2009). Glioma stem cell lines expanded in adherent culture have tumor-specific phenotypes and are suitable for chemical and genetic screens. Cell Stem Cell *4*, 568–580.

Ren, B., Yu, Y.P., Tseng, G.C., Wu, C., Chen, K., Rao, U.N., Nelson, J., Michalopoulos, G.K., and Luo, J.H. (2007). Analysis of integrin alpha7 mutations in prostate cancer, liver cancer, glioblastoma multiforme, and leiomyosarcoma. J. Natl. Cancer Inst. *99*, 868–880.

Ricci-Vitiani, L., Pallini, R., Larocca, L.M., Lombardi, D.G., Signore, M., Pierconti, F., Petrucci, G., Montano, N., Maira, G., and De Maria, R. (2008). Mesenchymal differentiation of glioblastoma stem cells. Cell Death Differ. *15*, 1491–1498.

Ricci-Vitiani, L., Pallini, R., Biffoni, M., Todaro, M., Invernici, G., Cenci, T., Maira, G., Parati, E.A., Stassi, G., Larocca, L.M., and De Maria, R. (2010). Tumour vascularization via endothelial differentiation of glioblastoma stem-like cells. Nature *468*, 824–828.

Singh, S.K., Hawkins, C., Clarke, I.D., Squire, J.A., Bayani, J., Hide, T., Henkelman, R.M., Cusimano, M.D., and Dirks, P.B. (2004). Identification of human brain tumour initiating cells. Nature *432*, 396–401.

Son, M.J., Woolard, K., Nam, D.H., Lee, J., and Fine, H.A. (2009). SSEA-1 is an enrichment marker for tumor-initiating cells in human glioblastoma. Cell Stem Cell *4*, 440–452.

Sun, L., Hui, A.M., Su, Q., Vortmeyer, A., Kotliarov, Y., Pastorino, S., Passaniti, A., Menon, J., Walling, J., Bailey, R., et al. (2006). Neuronal and glioma-derived stem cell factor induces angiogenesis within the brain. Cancer Cell *9*, 287–300.

Vescovi, A.L., Galli, R., and Reynolds, B.A. (2006). Brain tumour stem cells. Nat. Rev. Cancer *6*, 425–436.

von der Mark, H., Williams, I., Wendler, O., Sorokin, L., von der Mark, K., and Pöschl, E. (2002). Alternative splice variants of alpha 7 beta 1 integrin selectively recognize different laminin isoforms. J. Biol. Chem. *277*, 6012–6016.

Wang, R., Chadalavada, K., Wilshire, J., Kowalik, U., Hovinga, K.E., Geber, A., Fligelman, B., Leversha, M., Brennan, C., and Tabar, V. (2010). Glioblastoma stem-like cells give rise to tumour endothelium. Nature *468*, 829–833.

Wang, Z., Park, H.J., Carr, J.R., Chen, Y.J., Zheng, Y., Li, J., Tyner, A.L., Costa, R.H., Bagchi, S., and Raychaudhuri, P. (2011). FoxM1 in tumorigenicity of the neuroblastoma cells and renewal of the neural progenitors. Cancer Res. *71*, 4292–4302.

Yao, C.C., Ziober, B.L., Squillace, R.M., and Kramer, R.H. (1996). Alpha7 integrin mediates cell adhesion and migration on specific laminin isoforms. J. Biol. Chem. *271*, 25598–25603.

Zhong, J., Paul, A., Kellie, S.J., and O'Neill, G.M. (2010). Mesenchymal migration as a therapeutic target in glioblastoma. J. Oncol. *2010*, 430142.

Zhu, Z.H., Yu, Y.P., Zheng, Z.L., Song, Y., Xiang, G.S., Nelson, J., Michalopoulos, G., and Luo, J.H. (2010). Integrin alpha 7 interacts with high temperature requirement A2 (HtrA2) to induce prostate cancer cell death. Am. J. Pathol. *177*, 1176–1186.

Ziober, B.L., Chen, Y.Q., Ramos, D.M., Waleh, N., and Kramer, R.H. (1999). Expression of the alpha7beta1 laminin receptor suppresses melanoma growth and metastatic potential. Cell Growth Differ. *10*, 479–490.

STAR★METHODS

KEY RESOURCES TABLE

REAGENT or RESOURCE	SOURCE	IDENTIFIER
Antibodies		
Rabbit polyclonal anti Nestin	Sigma	Cat#N5413; RRID:AB_1841032
NL637 Mouse monoclonal anti Nestin	R&D Systems	Cat#NL1259V
Mouse monoclonal anti GPAP (clone 1B4)	BD Pharmigen	Cat#560298; RRID:AB_1645412
Mouse monoclonal anti Sox2	Cell Signaling	Cat#3579; RRID:AB_2195767
Mouse monoclonal anti Musashi (clone 282613)	R&D System	Cat#MAB2628; RRID:AB_2235632
Rabbit polyclonal anti Laminin	Sigma	Cat#L9393; RRID:AB_477163
Mouse monoclonal anti CD31 (clone JC70A)	DAKO	Cat#M0823; RRID:AB_2114471
Mouse monoclonal anti ITGA7	This paper	N/A
Mouse monoclonal anti ITGB1, used for immunoprecipitation	Santa Cruz Biotech.	Cat#sc-51649; RRID:AB_629022
Rabbit monoclonal anti AKT [S473]	Cell Signaling	Cat#4058; RRID:AB_331168
Rabbit monoclonal anti PLK1	Cell Signaling	Cat#4513; RRID:AB_2167409
Rabbit polyclonal anti FAK	Cell Signaling	Cat#3285; RRID:AB_2269034
Rabbit monoclonal anti FAK [Tyr397]	Cell Signaling	Cat#8556S; RRID:AB_10891442
Rabbit monoclonal anti FoxM1	Cell Signaling	Cat#5436; RRID:AB_10692483
Rabbit monoclonal anti FoxO3a	Cell Signaling	Cat#12829
Rabbit monoclonal anti FoxO3a [Ser253]	Cell Signaling	Cat#13129
Rabbit monoclonal anti Src	Cell Signaling	Cat#2123; RRID:AB_2106047
Rabbit monoclonal anti Src [Tyr416]	Cell Signaling	Cat#6943; RRID:AB_10013641
Rabbit monoclonal anti Skp2	Cell Signaling	Cat#2652S; RRID:AB_11178941
Rabbit monoclonal anti p38	Cell Signaling	Cat#8690S; RRID:AB_10999090
Rabbit monoclonal anti p38 [thr 180/tyr 182]	Cell Signaling	Cat#4511; RRID:AB_2139682
Rabbit polyclonal anti ITGB1, used for western blot	Santa Cruz Biotech.	Cat#sc-8978; RRID:AB_2130101
Mouse monoclonal anti Cyclin B1	Santa Cruz Biotech.	Cat#sc-166757; RRID:AB_2072277
Goat polyclonal anti AKT1	Santa Cruz Biotech.	Cat#sc-1618; RRID:AB_630849
Mouse monoclonal anti p27	Santa Cruz Biotech.	Cat#sc-1641; RRID:AB_628074
Rabbit polyclonal anti ITGA7	Sigma	Cat#HPA008427; RRID:AB_1851823
Mouse monoclonal anti beta tubulin	Sigma	Cat#T4026; RRID:AB_477577
Mouse monoclonal anti GFAP	BD Biosciences	Cat#556330; RRID:AB_396368
PE Mouse monoclonal anti CD133/AC133	Milteny	Cat#130-098-826
PE Rat monoclonal anti CD49f (clone GoH3), used for FACS	BD Biosciences	Cat# 555736; RRID:AB_396079
Mouse monoclonal anti integrin alpha 6 (clone 4F10), used for FACS	Santa Cruz Biotech.	Cat#sc-53356 RRID:AB_1125158
APC Rat monoclonal anti CD49f (clone GoH3)	Biolegend	Cat#313616
Rat monoclonal anti CD49f (clone GoH3), used for blocking	BioLegend	Cat#313614
APC Mouse monoclonal anti ITGβ1	BD Biosciences	Cat# 561794
Mouse monoclonal anti ITGβ1	Millipore	Cat#MAB2079Z; RRID:AB_2233964
Mouse monoclonal anti human integrin alpha 3 (clone P1B5) used for blocking	Millipore	Cat#MAB1952Z RRID:AB_11213492
Mouse monoclonal anti human integrin alpha 3 (clone P1B5) used for FACS	Millipore	Cat#MAB1952P; RRID:AB_1586938
Mouse monoclonal anti Ki67	Dako	Cat#M7240

(*Continued on next page*)

Continued

REAGENT or RESOURCE	SOURCE	IDENTIFIER
PE Mouse monoclonal anti EphA2 (clone 371805)	R&D	Cat#FAB3035P; RRID:AB_11128496
APC Mouse monoclonal anti CD44	BD Biosciences	Cat# 560890
Mouse monoclonal anti CD44 (clone DF1485)	DAKO	Cat#M7082; RRID:AB_2076596
Mouse monoclonal anti ITGA7	Miltenyi Bioteck	Cat#130-103-774
Mouse monoclonal anti murine ITGA7 (clone 6A11)	Acris	Cat#AM20012AF-N;
Please See Table S3 for Reverse Phase Protein Microarray Antibodies used	N/A	N/A
Biological Samples		
GSC (Glioblastoma Stem Cells)	(Marziali et al., 2016; Ricci-Vitiani et al., 2008)	N/A
Chemicals, Peptides, and Recombinant Proteins		
EGF	Peprotech	Cat#100-15
bFGF	Peprotech	Cat#100-18B
Apotransferrin	Sigma	Cat#T2252
Putrescine	Sigma	Cat#P5780
Sodium Selenite	Sigma	Cat#S5261
Bovine Serum Albumin	Sigma	Cat#A2153
Progesterone	Sigma	Cat#P8783
Insulin	Sigma	Cat#I3536
HAT Supplement 50X	Thermo Scientific	Cat#21060017
HT Supplement 100X	Thermo Scientific	Cat#11067030
BM Condimed H1 Hybridoma Suppl. 10X	Roche	Cat#11088947001
Matrigel	BD Biosciences	Cat#354230
Laminin	Sigma	Cat#L2020
Calcein AM	Sigma	Cat#C1359
Trypsin	Euroclone	Cat#ECM0920D
RNaseOUT Recombinant Ribonuclease Inhibitor	Thermo Scientific	Cat#10777019
GSK690693 AKT Inhibitor	Sigma	SML0428; CAS 937174-76-0
MK2206 AKT Inhibitor	Enzo Life Technologies	ENZ-CHM164-0005; CAS 1032350-13-2
SB203580 P38 Inhibitor	Enzo Life Technologies	BML-E1286-0001; CAS 152121-47-6
HOECHST 33342 Solution (RUO)	Biosciences	Cat#561908
Cell-tracker Oregon green 488	Thermo Scientific	Cat#C34555
7-Aminoactinomycin D	Sigma	Cat#A9400; CAS: 7240-37-1
SYBR Select Master Mix	Thermo Scientific	Cat#4472908
TaqMan Universal Master Mix II, no UNG	Thermo Scientific	Cat#4440040
M-MLV Reverse Transcriptase	Thermo Scientific	Cat#28025013
TRIzol Reagent	Thermo Scientific	Cat#15596018
Critical Commercial Assays		
Cell Titer Glo	Promega	Cat#G7571
Caspase 3/7 Glo	Promega	Cat#G8090
Myelin Removal Beads II	Miltenyi Bioteck	Cat#130-096-733
Deposited Data		
Mass spectrometric data obtained from the 1.4A12 immunoprecipitation	PRIDE (PRoteomics IDEntifications) data repository EMBL-EBI	PRIDE: PXD006069
Experimental Models: Cell Lines		
X63-Ag8.653	Gift from Prof. Peter H. Krammer, DKFZ Heidelberg	N/A
T98G	ATCC	ATCC: CRL-1690

(*Continued on next page*)

Continued

REAGENT or RESOURCE	SOURCE	IDENTIFIER
HEK293T	Gift from Dr. Till Wenger	N/A
L929	ATCC	ATCC: CCL-1
U87MG	ATCC	ATCC: HTB-14
HELA	ATCC	ATCC: CCL-2
Normal Human Neural Progenitor Cells	Lonza	PT-2599
Experimental Models: Organisms/Strains		
Balb/C mice	Harlan S.r.l Italy, now ENVIGO	Order Code 162
NSG NOD.Cg-Prkdcscid Il2rgtm1Wjl/SzJ mice	The Jackson Laboratory	Stock: 005557
NOD/Scid mouse NOD.CB17-Prkdc/NCrHsd mice	Harlan S.r.l Italy, now ENVIGO	Order Code 170
Oligonucleotides		
Primers for Real Time PCR, see methods Table S2	This paper	
Recombinant DNA		
pTWEEN	(Bonci et al., 2003)	N/A
pGL3 plasmid for pTWEEN-LUC-GFP generation	Promega	Cat#E1751
cDNA ITGA7	GE Lifesciences	Cat#BC050280
cDNA ITGA6	GE Lifesciences	Cat#BC136456
pLOC- ITGB1	GE Lifesciences	Cat#PLOHS_100003699
shRNA human pLKO.1 CTRL shRNA	GE Lifesciences	Cat#RHS4080
shRNA human pLKO.1 ITGA7 shRNA#1: AAAGGTAGCAAATCCCGGAGG	GE Lifesciences	Clone ID: TRCN0000057712
shRNA human pLKO.1 ITGA7 shRNA#2: ATCTAACACATAGTCCAGGGC	GE Lifesciences	Clone ID: TRCN0000057709
shRNA human pLKO.1 integrin β1 shRNA#1: TACATTCTCCACATGATTTGG	GE Lifesciences	Clone ID: TRC0000029646
shRNA human pLKO.1 integrin β1 shRNA#2: ATATCAGCAGTAATGCAAGGC	GE Lifesciences	Clone ID: TRC0000029645
psPAX2	Addgene	Cat#12260
pMD2.G	Addgene	Cat#12259
Software and Algorithms		
FlowJo v8.0	FlowJo, LLC	https://www.flowjo.com/
ELDA	(Hu and Smyth, 2009)	http://bioinf.wehi.edu.au/software/elda
IMAGEJ 1.46q	NIH	https://imagej.nih.gov/ij/index.html
GraphPad Prism 6.01	GraphPad Software	https://www.graphpad.com/
TCGA microarray data source	Brennan et al., 2013; Platform: Affymetrix Human U133A	https://cancergenome.nih.gov/
Source of the Sun glioma dataset	(Sun et al., 2006)	https://www.ncbi.nlm.nih.gov/geo/, GEO: GSE4290
Source of the REMBRANDT microarray data	(Madhavan et al., 2009)	http://www.betastasis.com/glioma/rembrandt/
GlioVis	(Bowman et al., 2017)	http://gliovis.bioinfo.cnio.es/
Other		
HiTrap MabSelect SuRe	GE Healthcare	Cat# 11-0034-94
Fluoroblock	BD Biosciences	Cat#351164
Paraformaldehyde	Sigma	Cat#P6148
Poly-L-lysine	Sigma	Cat#P5899
QIFIKIT	DAKO	Cat#K0078
T-PER	Pierce	Cat#78510

CONTACT FOR REAGENT AND RESOURCES SHARING

Additional information and requests for reagents may be directed to, and will be satisfied by, the Lead Contact, Ruggero De Maria at the Department of Pathology, Catholic University "Sacro Cuore," Rome. Email: ruggero.demaria@unicatt.it.

ANIMAL STUDIES

All animal procedures were performed according to the Italian National Animal Experimentation Guidelines (D.L.116/92) upon approval of the experimental protocol by the Institutional Animal Experimentation Committee.

Mouse strains used

For subcutaneous xenograft models we used six-week-old female NSG mice (NOD.Cg-Prkdcscid Il2rgtm1Wjl/SzJ; The Jackson Laboratory).

For intracranial (orthotopic) xenograft models we used six-week-old male NOD/Scid (NOD.CB17-Prkdc/NCrHsd, Harlan Laboratories Inc. Italy, now ENVIGO).

For the generation of the antibody library we used six-week-old female BALB/c (OlaHsd), Harlan Laboratories Inc. now ENVIGO).

Detailed description of the mouse models

For the subcutaneous tumor models, either $1x10^5$ GSC1 and GSC83 cells expressing integrin alpha 7 shRNA (Thermo Scientific) or $5x10^5$ luciferase expressing GSC1, GSC23c, GSC3 cells (Marziali et al., 2016; Ricci-Vitiani et al., 2008) were injected in (6-8 weeks old) female NSG mice (NOD.Cg-Prkdcscid Il2rgtm1Wjl/SzJ; The Jackson Laboratory). Cells were suspended 1:1 in matrigel (BD Biosciences; cat# 354263) and placed into the flanks of the mice (n = 12/group). The animals were treated ip with anti 1.4A12 (anti-ITGA7) or isotype control (BioXCell Cat#BE0085) at 10mg/kg twice weekly for 4 to 8 weeks.

For the orthotopic model, 6-8 weeks old male NOD/Scid (NOD.CB17-Prkdc/NCrHsd, Harlan Laboratories Inc. Italy, now ENVIGO) mice were anesthetized by ip injection of diazepam (2 mg/100 g) followed by intramuscular injection of ketamine (4 mg/100 g). Luciferase expressing GSCs were sorted for 1.4A12 (ITGA7) high and low expressing cells (0 passages in culture) and $1x10^4$ (GSC1) or $5x10^4$ (GSC1) and $2.5x10^3$ (GSC23c) were suspended in 3 μl DMEM-F12 (Invitrogen) and injected using a small animal stereotactic device (2 mm right of the midline and 1 mm anterior to the coronal suture). Tumor growth was monitored 3-6 months after injection by in vivo bioluminescence measurement. To this end, mice were ip injected with 150 mg/kg Luciferin (Perkin Elmer #122796) and after 12 min the bioluminescence was detected using an IVIS 100 small animal in vivo imaging system (PerkinElmer, former Xenogen).

For the assessment of in vivo antibody function upon orthotopic engraftment, 6 week old male NOD/Scid mice (NOD.CB17-Prkdc/NCrHsd, Harlan Laboratories Inc. Italy, now ENVIGO) were intracranially implanted with $2x10^5$ green fluorescence protein (GFP)-expressing GSCs suspended in 5 μl serum-free DMEM (Invitrogen) containing 3 μg anti-ITGA7 (this paper). Control mice were injected with equal numbers of GSCs suspended in 5 μl serum-free DMEM containing 3 μg isotype control mAb (IgG2a) (BioXCell Cat#BE0085). After grafting, the animals were kept under pathogen-free conditions in positive-pressure cabinets (Tecniplast S.p.A., Varese, Italy) and observed daily for neurological signs. Starting from the day of implantation, animals received anti-ITGA7 antibody (this paper; 10 mg/kg in 200 μl PBS) twice-weekly ip for 4 weeks. Control animals were treated with an equal concentration of isotype control antibody (BioXCell Cat#BE0085) ip After 8 weeks, the mice were deeply anesthetized and transcardially perfused with PBS (pH 7.4), followed by 4% paraformaldehyde (Sigma) in PBS for immunoistochemistry analysis.

Cell Lines

The GSCs from different patients were published before (Marziali et al., 2016; Ricci-Vitiani et al., 2008). All the lines were generated as reported before (Galli et al., 2004) and cultured in basal neuronal stem cell medium containing DMEM-F12 (GIBCO 52100-047; GIBCO 21700-018), 0.6% Glucose (Sigma, G8769), 0.11% sodium bicarbonate (Sigma, S8761), 5 mM HEPES (Sigma, H0887), 2 mg/L heparin (Calbiochem, 375095), 0.4% BSA (Sigma, A2153), 10% glutamine (Lonza, BE17-605E) and Penicillin/Streptomycin (Euroclone, ECB3001B). The basal medium was supplemented with 20 ng/ml EGF (Peprotech, 100-15), 10 ng/ml bFGF (Peprotech, 100-18B) and 10% Hormone mix (containing 20% DMEM-F12 5x conc (GIBCO), (0.6% Glucose (Sigma), 0.11% sodium bicarbonate (Sigma), 5 mM HEPES (Sigma), 1 g/L apotransferrin (Sigma, T2252), 50 mg/L insulin (Sigma, 91077C), 96.6 mg/L putrescine (Sigma, P5780), 0.3 μM sodium selenite (Sigma, S5261)). Cultures were expanded by mechanical dissociation of spheres followed by re-plating of both single cells and residual small aggregates in complete fresh medium. All GSC lines were kept between 10-15 passages in culture. The myeloma cell line X63-Ag8.653, T98G (ATCC, CRL-169), HeLa (ATCC, CCL-2) were maintained in RPMI 1640 (Euroclone ECM2001L), whereas HEK293T (gift of Dr. Till Wenger, DKFZ, Heidelberg), L929 (ATCC, CCL-1) and U87MG cell lines (ATCC, HTB-14) were cultivated in Dulbecco's modified Eagle's medium (Euroclone, ECM0728L) and incubated at 37°C, 5% CO_2 and supplemented with 10% fetal bovine serum (Euroclone). For the differentiation of primary GSC lines, GSCs were suspended in DMEM-F12 (Euroclone, ECM0095) containing 10% FBS, plated onto matrigel (BD Biosciences, 354230) coated 6 well plates at 50,000 cells/well and incubated for 10-14 days at 37°C, 5% CO_2.

METHOD DETAILS

Hybridoma generation

For the generation of the integrin alpha 7 specific antibody 1.4A12, female 6-week old BALB/c mice (OlaHsd) mice (Harlan Laboratories Inc. now ENVIGO) were immunized by ip injections of $5x10^5$ living GSC1 cells (> 10 passages in culture) (Marziali et al., 2016; Ricci-Vitiani et al., 2008) without adjuvant. 40, 70 and 84 days after the initial immunization, the antibody production was boosted by ip injection of $1\text{-}2x10^5$ GSC1. The final boost was performed as intra-venous (i.v.) injection using 50 μg protein from a membrane protein preparation of GSC1 cells. Subsequently the mice were euthanized, the spleen was removed under aseptic conditions and the splenocytes were fused with X63-Ag8.653 myeloma cells (generous gift from Prof. Peter H. Krammer, DKFZ Heidelberg) using standard fusion methods. One day after fusion the cells were directly plated in 96 well plates to densities of 1 to 5 surviving hybridoma clones/well (3000 wells/complete spleen) and selected with HAT supplement (ThermoFisher Scientific, Cat#21060017). After 10 days of HAT selection the hybridoma supernatants were tested for immunoreactivity toward primary brain tumor stem cells as described in the following section. Positive hybridomas were subcloned in HT supplement (ThermoFisher Scientific, Cat#11067030) containing medium twice and immunoreactivity was confirmed by flowcytometric analysis of antibody surface binding on GSC1. The hybridomas were frozen and stocked in nitrogen. Antibody purification was performed using a Hi-Trap MabSelect SuRe (GE Healthcare).

High throughput hybridoma screening

Peripheral-blood lymphocytes (PBL) and in vitro differentiated GSC1 cells were incubated with 10 μg/ml cell-tracker oregon green 488 (Thermo Scientific, Cat# C34555) and HOECHST 33342 (SIGMA #B2261), respectively for 20 min at 37°C. The unbound fraction of the dye was removed with 3 washes in PBS. The cells were then mixed in a 1:1:1 ratio with a single cell suspension of non-labeled GSC1 cells. The staining was performed in 96 well round bottom plates and 20,000 cells/well were incubated with 80 μl of the individual hybridoma supernatants for 1 hr on ice. The cells were washed twice with PBS 0.5% BSA. The bound antibody was then labeled with a PE-conjugated anti-mouse IgG (H+L) secondary antibody (ThermoFisher Scientific #P-852). The secondary antibody was diluted 1:200 in PBS 0.5% BSA and incubated for 30 min on ice. After washing, FACS analysis was performed using a LSR II flow cytometer equipped with a HTS-96 plate holder (Becton Dickinson). This methodology allowed for the analysis of more than 600 supernatants per day. The hybridomas, which produced antibodies binding preferentially to stem-like GSC1 but weakly or not to PBL were further analyzed for binding on other GSC or differentiated lines.

Microarray Database Analyses

Raw microarray data (Affymetrix Human U133A platform) were downloaded from The Cancer Genome Atlas (TCGA) repository (https://tcga-data.nci.nih.gov/publications/tcga) (Brennan et al., 2013). Raw data from a second study on glioma samples (Sun et al., 2006) were downloaded from the GEO database (https://www.ncbi.nlm.nih.gov/geo/, GEO: GSE4290). This dataset consisted of microarray data for 107 tumor samples (26 astrocytoma and 81 glioblastoma) and 23 non-tumor samples from epilepsy patients from the Affymetrix Human U133 Plus 2.0 Array. For the data of The National Cancer Institute's Repository for Molecular Brain Neoplasia dataset (REMBRANDT) (https://caintegrator.nci.nih.gov/rembrandt) the cutoff was set at < 0.5 fold of the mean expression for patients expressing low levels of ITGA7. For the other datasets we took advantage of the online tool GlioVis (http://gliovis.bioinfo.cnio.es/) and analyzed the data with GraphPad software.

Immunoprecipitation

For the preparative immunoprecipitation experiments, $5x10^7$ GSC1 cells were lysed in 1 mL IP-lysis buffer (30 mM Tris-HCl [pH 7.4], 120 mM NaCl, 2 mM EDTA, 2 mM KCl, 1% Triton X-100, plus protease- inhibitor cocktail [Roche, 04906837001]) at 4°C for 30 min. The lysates were centrifuged at 15,000 × g for 30 min. Preclear was performed two times with magnetic protein G beads (Invitrogen) in presence of 5 μg isotype control antibody (IgG2a) (Southern Biotech, 0103-01) and one time with magnetic protein G beads alone for 30 min/each. ITGA7 was precipitated using 1.4A12 antibody (this paper) for 4 hr at 4°C. The beads were washed five times with 1 mL IP-lysis buffer and eluted with 2 × LDS buffer (Invitrogen, NP0007). Proteins were separated by SDS-PAGE and analyzed by silver staining and Coomassie staining. For the analytical immunoprecipitation, $2x10^6$ GSC1 cells were surface biotinylated with Sulfo-NHS-LC-Biotin (Pierce/Thermo Fisher) according to the manufacturers' protocol. Immunoprecipitation was performed as described above and the biotinylated proteins were detected by western blot using streptavidin-HRP (GE Healthcare, RPN1231VS). Rabbit polyclonal anti ITGB1 antibody (Santa Cruz Biotech. Biotech., *sc-8978*) was used for ITGB1 immunoprecipitation.

Mass spectrometry

1D PAGE gel pieces were washed with 150 μl water for 5 min at 37°C. Proteins were reduced with DTT, alkylated with 100 μl 55 mM iodoacetamide in 40 mM NH_4HCO_3 for 30 min at 25°C, followed by three alternating washing steps each with 150 μl of water and water/acetonitrile. Gel pieces were then dehydrated with 100 μl neat acetonitrile for 1 min at room temperature, dried for 15 min and rehydrated with porcine trypsin (170 ng trypsin in 10 μL 40 mM NH4HCO3, sequencing grade, Promega). After overnight digestion at 37°C the supernatant was collected while gel pieces were subjected to three alternating 0.1% TFA and acetonitrile/0.1% TFA 50:50 (v/v) extraction steps. The combined solutions were evaporated, and redissolved in 0.1% TFA for MS analysis. Peptides were separated using a nano Acquity UPLC system (Waters GmbH). Peptides were trapped on a nano Acquity C18 column, 180 μm x 20 mm, particle size 5 μm and separated on a C18 column (BEH 130 C18 100 μm x 100 mm, particle size 1.7 μm (Waters GmbH)

with a flow rate of 400 nl/min. The chromatography was carried out using a 1h gradient of solvent A (98.9% water, 1% acetonitrile, 0.1% formic acid) and solvent B (99.9% acetonitrile and 0.1% μl formic acid) in the following sequence: from 0 to 4% B in 1 min, from 4 to 40% B in 40 min, from 40 to 60% B in 5 min, from 60 to 85% B in 0.1 min, 6 min at 85% B, from 85 to 0% B in 0.1 min, and 9 min at 0% B. The nanoUPLC system was coupled online to a LTQ Orbitrap XL (Thermo Scientific). The Orbitrap was operated with the following parameters: ESI voltage 2400V; capillary temperature 200°C, normalized collision energy 35 V. The Orbitrap scan resolution was set to 60000 at m/z 400 and the mass range from m/z = 200 to 2000. Six MS/MS scans of the most abundant precursor ions were acquired in the LTQ scan cycles. MASCOT search engine (Matrix Science), version 2.4 against SwissProt database 2017_02 (553655 sequences; 198177566 residues) was used for protein identification. The peptide mass tolerance was set to 5 ppm and fragment mass tolerance to 0.4 Da. Carbamidomethylation of C was set as fixed modification. Variable modifications included oxidation of M and deamidation of NQ. One missed cleavage site in case of incomplete trypsin hydrolysis was allowed. Proteins were considered as identified if more than one unique peptide had an individual ion score exceeding the MASCOT identity threshold (ion score cut-off of 26-27). Identification under the applied search parameters refers to False Discovery Rate (FDR) < 1.5% and a match probability of $p < 0.01$, where p is the probability that the observed match is a random event. The raw data obtained by mass spectrometry were deposited in the PRIDE (PRoteomics IDEntifications) data repository of the EMBL-EBI with the dataset identifier PRIDE: PXD006069.

Lentiviral constructs

All ectopic expression experiments were performed with lentiviral transduction using pRRL-CMV-PGK-EGFP-WPRE called pTWEEN (Bonci et al., 2003). The open reading frame of ITGA7 was purchased as cDNA GE Lifesciences (Open biosystems) and shuttled via PCR cloning in the pTWEEN (ITGA7 for: agctcgcgcagggatcgtccc; ITGA7 rev: gccgatcctgccaaatcttgatgcg). The lentiviral reporter vector TWEEN-LUC-GFP was constructed by using pTWEEN as a backbone for subcloning a firefly luciferase NheI/XbaI cDNA fragment extracted from pGL3 (Promega) into the XbaI site at the 3′ of the CMV promoter. The lentiviral expression vector for ITGB1 (pLOC) was purchased from GE Lifesciences (Open biosystems). The shRNA containing vectors are pLKO.1 based and were purchased from GE Lifesciences (Open biosystems).

HEK293T cells were co-transfected with the packaging vector (psPAX2, ADDGENE), the envelope vector (pMD2.G, ADDGENE) and the expression construct (pLKO.1 or pTWEEN). For transfection we used standard CaPO4 transfection methods according to the manufacturer's recommendation (CalPhos, Clontech, Mountain View, CA).

Whole brain reconstructions and tumor cells invasion analysis

To analyze the GBM stem cells invasion after isotype control and 1.4A12 antibodies treatments IF was performed on an intracranial xenografts model of NOD/Scid mice (NOD.CB17-Prkdc/NCrHsd, Harlan Laboratories Inc. now ENVIGO). Mice were deeply anesthetized and transcardially perfused with saline followed by 4% paraformaldehyde in 0.1 M phosphate buffer pH 7.4. The brain was removed, stored in 30% sucrose buffer at 4°C until it sank, embedded and frozen in OCT and serially cut at 20 μm on the coronal plane. Sections were collected in distilled water, mounted on slides, and coverslipped with Vectashield mounting medium (Vector Laboratories, USA). For the whole brain reconstructions about 70 photomicrographs for every single brain sections were obtained with a Zeiss Axiophot fluorescent microscope equipped with a Zeiss MRC Axiocam. Every reconstruction was obtained merging all single images using Photomerge tool of Photoshop software (Adobe, USA). The distance traveled into the brain parenchyma from tumor bulk by single tumor cells, in control and α−ITGA7 treated mice, was measured using Zeiss Axiovision software. In particular, the cranio-caudal extension of the brain area invaded by GFP-expressing GSCs was assessed on serial coronal sections. Then histological sections were digitized and on each image the brain region containing GFP^+ cells was demarcated with the cursor and its area calculated (IMAGEJ 1.46q; available at https://imagej.nih.gov/ij/index.html). To assess the tumor volume, each area of infiltrated brain was multiplied for the distance to the consecutive digitized section starting from the tumor epicenter to the cranial and caudal poles of the tumor and partial volume values were added. The number of GFP^+ tumor cells in the corpus callosum and anterior commissure contralateral to the grafted striatum was also assessed. In each specimen, at least five and three sections passing through the corpus callosum and anterior commissure, respectively, were averaged.

Immunofluorescence Microscopy

After fixation with 4% PFA, the tumor spheres where seeded on round coverglasses coated with poly-L-lysine (Sigma, P5899) and allowed to attach for 10 min at RT. Differentiated cells were directly grown on the matrigel (BD Biosciences, 354230) coated coverglasses for 14 days at 37°C before fixation and permeabilization. Prior the incubation with antibodies, the cells were blocked with a PBS solution containing 3% BSA (Sigma) plus 0.05% TWEEN20 (Sigma, P1379) for 1 hr at RT. Samples were then incubated overnight with the primary antibody and rinsed with PBS three times before incubation with secondary antibodies and 10μg/ml DAPI (Life technologies, D1306) for 3 hr at RT. Following 3 rinses in PBS, the slides were mounted with ProLong Gold AntiFade Reagent (Thermo Fisher Scientific, P36930) and imaging was performed with a FV1000 Olympus spectral confocal microscope (equipped with a 20X, 40X and 60X plan-apochromatic high N.A. objectives). Antibodies used were anti integrin α7 (1.4A12 purified antibody or surnatant, this paper), rabbit polyclonal anti-Nestin (Sigma, N5413), anti- GFAP (BD Pharmigen, 560298, clone 1B4), anti-Sox-2 (Cell Signaling, D6D9), anti-Musashi (RD System, MAB2628, clone282613), polyclonal rabbit anti-Laminin (Sigma, L9393), anti CD31 (DAKO, M0823, clone JC70A) and anti Ki67 (DAKO #M7240). After accurately rinses the following secondary antibodies were used: goat anti mouse IgG2a Alexa555-conjugated (Life Technologies, A21121), goat anti mouse IgG1 Alexa488-conjugated (Life Technologies, A21137) and goat anti rabbit IgG Alexa647-conjugated (Life Technologies, A21244).

Surgical human GBM biopsy specimens and GBM cell samples were fixed overnight in 4% PFA at 4°C, stored in 30% sucrose buffer overnight at 4°C and cryosectioned (OCT embedded). Sections were blocked with a PBS solution containing 3% BSA (Sigma) plus 0.05% TWEEN20 for 1 hr at RT. The following primary antibodies (1:200 dilution) were incubated ON at 4°C: mouse monoclonal anti CD31 (DAKO, M0823, clone JC70A), mouse monoclonal anti integrin α7 (1.4A12 antibody, this paper), rabbit polyclonal anti Laminin (Sigma, L9393), Ki67 (DAKO M7240, clone MIB-1). After washing secondary antibodies were used goat anti mouse IgG2a Alexa555-conjugated (Life Technologies, A21121) and goat anti rabbit IgG Alexa647-conjugated (Life Technologies, A21244). After the sections were washed 3 times with PBS and incubated with secondary antibodies and 10μg/ml DAPI (Life technologies, D1306) for 3 hr at RT. After 3 washing in PBS, the slides were mounted with ProLong Gold AntiFade Reagent (Thermo Fisher Scientific, P36930). The images were were acquired with a Laser scanning confocal microscope (FV1000 Olympus equipped with a 20X, 40X and 60X plan-apochromatic high N.A. objectives). To perform immunofluorescence microscopy on subcutaneous xenografts the mice were deeply anesthetized and subcutaneous xenografts were removed 12 weeks after grafting. The specimens were fixed in 4% PFA for 12 hr. The specimens were cryoprotected in 30% sucrose buffer for 48 hr at 4°C then serially cryosectioned at 40 μm. Free floating sections were permeabilized with PBS 0.5% Triton X-100 (Sigma) solution for 45 min at RT and blocked with a PBS 3% bovine serum albumin (BSA) for 45 min at RT. After PBS rinses, samples were incubated with primary antibodies against Ki67 (rabbit monoclonal 91061, 1:100, Thermo-Scientific, USA), p-FAK (Tyr397) (rabbit monoclonal D20B1, 1:150, Cell Signaling #8556) and p-AKT (Ser473) (rabbit monoclonal 193H12, 1:200, Cell Signaling #4058) overnight at 4°C. After three rinses in PBS, sections were incubated with DyLight 549 Goat anti-Rabbit IgG (1:200, Vector Laboratories, USA) as secondary antibodies, for 45 min RT. After washing, sections were coverslipped using Vectashield mounting medium with DAPI (Vector Laboratories, USA). Confocal images were generated using a Zeiss 510 Meta confocal microscope.

Real-Time PCR

Total RNA was extracted from GSC xenografts high and low 1.4A12 sorted cells and primary GBM cells (max 15 passages in culture) upon ITGA7 knockdown, using TRIZOL reagent (Thermo Scientific). RNA was extracted according to the manufacturer's instruction. RNA was reverse transcribed to cDNA using M-MLV Reverse Transcriptase (Thermo Scientific) according to the manufacturer's instructions. qPCR reactions were performed using an StepOne Plus system (Thermo Scientific) using SYBR Master Mix (Thermo Scientific) and TaqMan Master Mix (Thermo Scientific). qRT-PCR was performed for various genes of interest. The primers used can be found in Table S2 related to the STAR Methods. Results were normalized to GAPDH levels. Data were analyzed by StepOne Plus Software v2.3 and Excel.

Western Blotting

Protein lysates were prepared using standard RIPA buffer (150 mM NaCl; 20 mM Tris, pH 7.2; 0.05% SDS; 1.0% Triton X-100; 1% Deoxycholate; 5 mM EDTA) plus protease-phosphatase inhibitor cocktail (Roche, 04906837001; 04693124001). The proteins were separated with NuPAGE gels (Invitrogen). For the laminin attachment lysates preparation, 6 wells plate were coated ON at 4°C and for additional two hours at 37°C with 10 μg/ml laminin (Sigma). After the wells were washed 3 times with PBS. 5x 10^5 wild-type GSC cells, mechanically dissociated, were pretreated for 20 min at 37°C with PBS, isotype ctrl or 1.4A12 antibodies (10μg/ml). After the cells were plated for the indicated time points at 37°C and lysed on ice. Same procedures it was applied for GSC ITGA7 knockdown cell lysates preparation. Proteins were blotted according to the manufacturers' recommendation (Invitrogen). The nitrocellulose membranes (GE Healthcare, 10600018) were blocked for 1 hr with PBS-T (PBS, 0.02% TWEEN20) containing 5% blotting grade not-fat powdered milk (Euroclone, 180500).

The following primary antibodies were used 1 to 1,000 in PBS containing 3% BSA and incubated overnight at 4°C: rabbit monoclonal anti p-AKT (S473) (Cell Signaling, 4058), Rabbit monoclonal anti PLK1 (Cell Signaling, 4513), rabbit polyclonal anti FAK (Cell Signaling, 3285), rabbit monoclonal anti p-FAK (Y397) (Cell Signaling 8556), rabbit monoclonal anti FoxM1 (Cell Signaling, 5436), rabbit monoclonal anti FoxO3a (Cell Signaling, 12829), rabbit monoclonal anti p-FoxO3A (S253) (Cell Signaling, 13129), rabbit monoclonal anti Src (Cell Signaling, 2123), rabbit monoclonal anti p-Src (Tyr416) (Cell Signaling, 6943), mouse monoclonal anti Sox2 (Cell Signaling, 3579), rabbit monoclonal anti Skp2 (Cell Signaling, 2652), rabbit monoclonal anti p38 (Cell Signaling, 8690), rabbit monoclonal anti p-p38 (Thr 180/Tyr 182) (Cell Signaling, 4511), rabbit polyclonal anti ITGβ1 (Santa Cruz Biotech. Biotech., sc-8978), mouse monoclonal anti Cyclin β1 (Santa Cruz Biotech. Biotech., sc-166757), goat polyclonal anti AKT1 (Santa Cruz Biotech. Biotech., sc-1618), mouse monoclonal anti p27 (Santa Cruz Biotech. Biotech., sc-1641), rabbit polyclonal anti ITGA7 (SIGMA, HPA008427); mouse monoclonal anti beta tubulin (SIGMA, T4026). The isotype specific secondary antibodies used were obtained from Southern Biotechnologies and diluted 1:10,000 in PBST containing 0.5% milk at room temperature. After chemiluminescent detection (Euroclone, EMP01105; GE Healthcare RPN2236), membranes were washed and a reblot was eventually performed by rinsing with a 50 mM glycine buffer at pH 2.3 for 10-15 min.

Flow Cytometric Analysis

Cells were mechanically dissociated, washed and suspended in PBS/BSA 0,5% buffer. For the intracellular staining the cells were fixed in 200 μL PBS containing 2% PFA for 10 min and permeabilized with PBS/Triton 0.1%. Primary antibody was diluted in PBS/Triton 0.1% and the cells were stained 45 min on ice. After two washes in PBS Triton 0.1% at 4°C, cells were incubated with secondary antibody in PBS/Triton 0.1% for 30 min on ice. Finally, the cells were washed and suspended in 100 μL PBS BSA 0.5% and analyzed by flow cytometry. For extracellular stainings, intact cells were incubated for 45 min with primary antibody in PBS

BSA 0.5% or in hybridoma SN. Cells were washed twice in PBS/BSA 0.5% and incubated with the secondary antibody in PBS BSA 0.5% for 30 min. Viable cells were detected by 7-Amino-actinomycin D (Sigma, A9400) exclusion. The results were analyzed with FloJo software (https://www.flowjo.com/). Antibodies used were: mouse monoclonal anti GFAP (BD Biosciences, 556330), rabbit polyclonal anti ITGB1 (Santa Cruz Biotech., sc-51649), PE mouse monoclonal anti CD133/AC133 (Miltenyi, 130-098-826), PE rat monoclonal anti CD49f (BD Biosciences, 555736, clone GoH3), NL637 Mouse monoclonal anti Nestin (R&D Systems, NL1259V) and mouse monoclonal anti-ITGA7 (1.4A12 antibody, this paper), mouse monoclonal anti EphA2 (R&D, FAB3035P, clone 371805), APC Mouse monoclonal anti CD44 (BD Biosciences, 560890) For the determination of ITGA molecules on the cell surfaces QIFIKIT (DAKO, K0078) was used as recommended by the manufacturer using mouse IgG antibodies: mouse monoclonal anti human ITGA3 (Millipore, MAB1952P clone P1B5), mouse monoclonal anti ITGA6 (Santa Cruz Biotech. Biotech., sc-53356, clone 4F10) and mouse monoclonal anti ITGA7 antibody (1.4A12 antibody, this paper).

Tissue Processing and Cell Sorting

Mice were euthanized by cervical translocation and the xenografted tumor was removed under sterile conditions. The tumor cells were isolated by mechanical dissociation using scalpel and micro-scissors. Then the cells were filtered with a 70 μm mesh before red blood cells were lysed using RBC lysisbuffer according to the manufacturers' recommendation (Miltenyi). Myelin was removed with myelin removal beads and MACS columns following the manufacturers' recommendation (Miltenyi) After successful myelin removal the cells were suspended at a density of $1x10^7$ cells/ml and stained with mAb 1.4A12 (10 μg/ml) or isotype control (BioXCell Cat#BE0085). mAb 1.4A12 high and low expressing cell populations were sorted using a FACS aria II (Becton Dickinson). After sorting the purity of the cell populations was controlled by flow cytometry using a FACS Canto (Becton Dickinson). When the purity was > 90% the cells were used for downstream applications without passaging in culture.

Cell Cycle Analysis

Cells were harvested and mechanically dissociated. Then the cells were lysed in 0.1 M citrate buffer pH 7.4 containing 0.1% Triton X-100, 50 μg/ml propidium iodide (Sigma) and 50 μg/ml RNaseA (Sigma) on ice for 30 min. Then samples were measured by flow cytometry and analyzed using FlowJo software https://www.flowjo.com/.

Cell Viability and Caspase 3/7 Assay

After plating equal number of cells, the Cell Titer-Glo® Luminescent Cell Viability Assay (Promega) and Caspase 3/7 Assay (Promega) was performed. Control wells containing medium without cells were prepared to obtain a value for background luminescence. We normalized the values obtained for each time point to day 0. If not described otherwise, the results are the means and standard error of the mean (SEM) of 3 to 5 independent experiments.

Limiting Dilution Assay

GSC cells were plated in 60 wells to 3, 10, 30 and, depending on the sample, 1 or 100 cells/well. GSC cells were incubated in basal neuronal stem cell medium supplemented with 80 ng/ml EGF and 40 ng/ml bFGF at 37°C. After 15 and 25 days 20 μl of medium containing 100 ng/ml EGF and 50 ng/ml bFGF was added to ensure the presence of GFs during the growth period. After 20-40 days the wells were controlled for vital colonies. These were counted and the clonogenic capacity was calculated using ELDA software (Hu and Smyth, 2009).

Invasion Assay

For the invasion assay the upper chambers of the Fluoroblok plate (BD Biosciences, 351164) were coated with 20 μg/ml laminin (Sigma, L2020) diluted in PBS for 3 hr at RT. Then the wells were washed 3 times with PBS. The lower chambers were filled with basal neuronal stem cell medium containing 60 ng/ml EGF and 30 ng/ml bFGF. $4x10^4$ cells were washed 3 times with PBS and suspended with basal neuronal stem cell medium and treated with the following concentration of antibodies: rat monoclonal antiCD49f (BioLegend, 313614, clone GoH3), mouse monoclonal anti human ITGA3 (Millipore, MAB1952Z, clone P1B5), mouse monoclonal anti ITGA7 (1.4A12 antibody, this paper), 1.4A12 F(ab) when indicated and rat isotype control (BioLegend, 400516, clone RTK2758) and IgG2a isotype control (BioXCell Cat#BE0085). The cells were incubated at 37°C for 48 hr. The cells were stained with 4μM calcein (Sigma) and analyzed with the fluorescence microscope. The microscopic pictures were then analyzed using ImageJ software, NIH, (https://imagej.nih.gov/ij/index.html). The antibody treatment was not influencing the cell viability in the 48 hr treatment period.

Reverse Phase Protein Microarrays

Control and integrin α7 knockdown cells were lysed in TPER (Pierce) plus Protease Inhibitor Cocktail (Sigma 04693132001) and Phosphatase Inhibitor Cocktail (Sigma #4906837001). RPPA analysis was performed using established procedures (Marziali et al., 2016). Image analysis for spot recognition, quantification and normalization was carried out using 'MicroVigene' v5.2 software http://www.vigenetech.com/MicroVigene.htm (VigeneTech Inc). Data analysis and generation of heatmaps and plots was carried out by means of 'R' v3.3.2 https://www.R-project.org/ (R Foundation for Statistical Computing) and 'RStudio' v1.0.136 https://www.rstudio.com/ (RStudio) using the following installed packages: plyr, dplyr, tidyr, ComplexHeatmap, ggplot2, RColorBrewer and shiny.

QUANTIFICATION AND STATISTICAL ANALYSIS DATA

All experiments were repeated at least three times. When not indicated otherwise, data were analyzed using the two-tailed Student's t test or one-way ANOVA, depending on number of groups compared. When one-way ANOVA was chosen, we performed Dunnett's multiple comparisons post hoc test to analyze the variances. For both methods a probability value of 0.05 or less was considered significant. Kaplan-Meier survival curves were analyzed by using Log-rank statistics comparing the different patient groups. The limiting dilution assays were analyzed by using ELDA software (http://bioinf.wehi.edu.au/software/elda).

Gene expression values as computed with RMA and analyzed by means of R (http://www.r-project.org/) and Prism 5 (GraphPad Software, Inc., CA) software. Following Shapiro-Wilk normality testing, differential expression levels in TCGA and GSE7696 dataset were tested by means of Mann-Whitney U test (Prism 5) for each selected gene. ITGA7 expression analysis in GBM subtypes in our TCGA dataset was carried out using Kruskal–Wallis one-way analysis of variance, with Dunn post hoc test (Prism 5), since different samples were homoscedastic and not-normally distributed (respectively Levene and Shapiro-Wilk tests, R software). R analysis on ITGA7 expression in the GEO: GSE4290 dataset showed that data were heteroscedastic and normally distributed, hence we performed a Welch ANOVA with Waller-Duncan K-ratio test for post hoc. For the survival analysis the patients were divided into an ITGA7 high (z-score > median) and an ITGA7 low expressing (z-score < median) group. OAS curves were analyzed using the Log-rank (Mantel-Cox) test (Prism 5) and the Cox proportional-hazards regression (R software).

DATA AND SOFTWARE AVAILABILITY

The accession number for the mass spectrometry data reported in this paper is PRIDE: PXD006069.

The list of software for data analysis and processing can be found in the Key Resources Table.